,			

ABSTRACT

STRUCTURAL AND PHASE INVESTIGATIONS

- I. CRYSTAL AND MOLECULAR STRUCTURE OF $\pi\text{-CYCLOPENTADIENYLBIS} (\texttt{ACETYLACETONATO}) \texttt{CHLOROZIRCONIUM}(\texttt{IV})$
 - II. NONSTOICHIOMETRY IN Sm(II)-Sm(III) FLUORIDES

BY

John Joseph Stezowski

The crystal structure of π -cyclopentadienylbis(acetylacetonato) chlorozirconium(IV), π -C₅H₅(C₅H₇O₂)₂ZrCl, which crystallizes with the symmetry of the monoclinic space group $P2_1/c$, has been determined by equi-inclination Weissenberg single crystal X-ray diffraction techniques. The theoretical density (1.553 g cm⁻³) calculated for four molecules per unit cell with the observed lattice parameters (a = 8.42 ± 0.01 , b = 15.66 ± 0.01, c = 15.17 ± 0.02 $^{\circ}$ A, β = 123025' ± 4') is in agreement with the measured value $(1.556 \pm 0.005 \text{ g cm}^{-3})$. The final discrepency factor, R = 0.092, results from a full matrix least squares refinement of visually estimated relative intensities for 1453 reflections (sin $\theta/\lambda \leq 0.54$, CuKa radiation). The observed dodecahedral stereochemical configuration of the molecule is compatible with π -bonding between the cyclopentadienyl ligand and the zirconium atom and also appears to allow $d_{\pi}-p_{\pi}$ interaction between B-oxygen and the zirconium atoms. Intermolecular forces within the lattice, which exhibits distinct layers, appear to be confined to van der Waals interactions.

A nonstoichiometric Sm(II)-Sm(III) system has been prepared by reacting varying amounts of samarium metal with samarium trifluoride. The system, SmF2 to SmF2 to SmF2 displays crystal lattice modifications of the fluorite unit cell exhibited by stoichiometric SmF2.00. A cubic phase which displays a regular decrease in its lattice parameters (a = 5.867 ± 0.001 to a = 5.841 ± 0.001 Å) as the composition is changed from $SmF_{2,100}$ to $SmF_{2,16}$, a tetragonal phase (a = 4.106 ± 0.002 and c = 5.825 ± 0.003 Å), SmF_{2.35}, and a rhombohedral phase, which also displays variable lattice parameters (a = $7.124 \pm 0.002 \text{ Å}$, $\alpha = 33.40 \pm 0.020 \text{ to a} =$ 7.096 \pm 0.002 Å, α = 33.23 \pm 0.02°) as the composition is varied from SmF2.41 to SmF2.46, have been found by Guinier powder X-ray diffraction techniques. The density-composition behavior of the system has been measured; the density increases as the F:Sm atomic ratio is varied from 2.00 to 3.00 and is compatible with an interstitial anion description of the lattice modifications. Several similarities between these fluorides and the UO2-UO3 system have been observed.

STRUCTURAL AND PHASE INVESTIGATIONS

- I. CRYSTAL AND MOLECULAR STRUCTURE OF $\pi\text{-CYCLOPENTADIENYLBIS} (\text{ACETYLACETONATO}) \text{CHLOROZIRCONIUM} (\text{IV})$
 - II. NONSTOICHIOMETRY IN Sm(II)-Sm(III) FLUORIDES

Ву

John Joseph Stezowski

A THESIS

Submitted to
Michigan State University
in partial fulfillment of the requirements
for the degree of

DOCTOR OF PHILOSOPHY

Department of Chemistry

1968



ACKNOWLEDGMENT

The author wishes to convey his sincere thanks to Dr. Harry A. Eick for his interest, encouragement, and support throughout the pursuit of this work.

Appreciation is extended to Dr. Alexander Tulinsky for the use of his equipment and to Dennis B. Shinn for his assistance in the early stages of this investigation.

The rapport among the members of the High Temperature Research Groups was particularly interesting and frequently a source of inspiration.

The author is grateful to the E. I. duPont de Nemours

Company for a duPont Teaching Fellowship. Financial assist
ance from the Department of Chemistry and the United States

Atomic Energy Commission is also gratefully acknowledged.

TABLE OF CONTENTS

PART I. CRYSTAL AND MOLECULAR STRUCTURE OF π -CYCLOPENTA-DIENYLBIS (ACETYLACETONATO)CHLOROZIRCONIUM(IV)

	Pa	age
I.	INTRODUCTION	1
II.	EXPERIMENTAL	6
	Crystal Properties	6 7
	Lattice Parameters and Density	10 12 14
	Computations	16
III.	STRUCTURE DETERMINATION	18
	Patterson Synthesis	18 24 26
IV.	DESCRIPTION OF THE STRUCTURE	33
	The Unit Cell	33 37
PART	II. NONSTOICHIOMETRY IN Sm(II)-Sm(III) FLUORIDES	
v.	INTRODUCTION	52
VI.	EXPERIMENTAL	55
	Preparation of Samarium Trifluoride Preparation of the Reduced Samarium Fluorides Vapor Transport Experiments	55 57 61 62 65 67

TABLE OF CONTENTS (Cont.)

		Page
VII.	RESULTS	69
	Samarium Trifluoride	69
	Fluorides	69 70 71 73 73
VIII.	DISCUSSION	80
	Fluorite Lattice	80 81 89 90
IX.	SUGGESTIONS FOR FUTURE RESEARCH	93
	BIBLIOGRAPHY	96
	APPENDIX I. Description of Computer Program .	100
	APPENDIX II. Parameters from the Anisotropic Refinement of the Structure of $\pi-C_5H_5\left(C_5H_7O_2\right)_2$ ZrCl	107
	APPENDIX III. Powder X-ray Diffraction Data for the Sm(II)-Sm(III) Fluorides	109

LIST OF TABLES

TABLE	PA	AGE
I.	Properties of space group $P2_1/c$ (No. 14)	11
II.	Crystal boundary planes and their distance from the origin within the crystal	16
III.	Positions and intensities of principle Patterson peaks	23
IV.	Electron density peak heights and assignments to atoms for π -C ₅ H ₅ (C ₅ H ₇ O ₂) ₂ ZrCl	25
v.	Dispersion corrections for zirconium	29
VI.	Atomic co-ordinates for $\pi\text{-C}_5\text{H}_5\left(\text{C}_5\text{H}_7\text{O}_2\right)_2\text{ZrCl}$.	31
VII.	Observed and calculated structure factors	32
VIII.	Selected interatomic bond lengths and angles.	40
IX.	Summary of interatomic parameters for some hexa-co-ordinate transition metal acetylacetonate complexes	41
х.	Samarium analysis and stoichiometry	72
XI.	Oxygen analyses obtained from National Spectrograph Laboratories (Cleveland, Ohio)	72
XII.	Density of reduced samarium fluorides	74
XIII.	Lattice parameters as a function of composition for a reduced samarium fluoride phase .	76
XIV.	Rhombohedral unit cell parameters as a function of composition	79
xv.	Comparison of the stoichiometries generated by $Sm_{12}F_{24+n}$ and those observed for phase boundaries	89

LIST OF TABLES (Cont.)

TABLE	I	PAGE
XVI.	Atomic co-ordinates for $\pi-C_5H_5(C_5H_7O_2)_2$ ZrCl from the structure refinement with anisotropic thermal parameters	107
XVII.	Anisotropic thermal parameters	108
XVIII.	<pre>Powder X-ray diffraction data for the cubic Sm(II)-Sm(III) fluorides</pre>	109
XIX.	Powder X-ray diffraction data for the samples in the cubic-tetragonal two-phase region	110
xx.	Powder X-ray diffraction data for the tetragonal $SmF_{2.35}$ with the superstructure lines also included	111
xxI.	Powder X-ray diffraction data for the rhombohedral Sm(II)-Sm(III) fluorides	112

LIST OF FIGURES

Figure		Page
1.	Crystals of π -C ₅ H ₅ (C ₅ H ₇ O ₂) ₂ ZrCl	8
2.	Optical extinctions	8
3.	Representation of space group $P2_1/c$	11
4.	Symmetry of the Patterson Map	21
	a) Symmetry of the $(u,1/2,w)$ plane b) Symmetry of the $(0,1/2,w)$ line	
5.	Comparison of weighting schemes	28
6.	Stereographic projection of the unit cell	34
7.	Stereographic projection of the unit cell	34
8.	Projections of the molecule	38
9.	Square antiprism	43
10.	Undecahedron	43
11.	Dodecahedron	44
12.	Projected co-ordinate angles for the octahedral undecahedron	47
13.	Projected co-ordinate angles for the general undecahedron	47
14.	Projected co-ordinate angles for the $\pi-C_5H_5\left(C_5H_7O_2\right)_2$ ZrCl	47
15.	Projected co-ordinate angles for the dodecahedron	47
16.	Schematic representation of the SmF ₃ preparation line	56

LIST OF FIGURES (Cont.)

Figure	Pa	age
17.	Schematic of Guinier Camera	63
18.	A typical film cassette-shrinkage correction for Guinier photographs	66
19.	Density of CH2Br2 as a function of temperature	74
20.	Estimated relative line intensity from powder pattern obtained from samples in the composition range SmF _{2.17} -SmF _{2.35}	77
21.	Density as a function of composition	82
22.	The effect of composition on the lattice parameter on the cubic samarium fluoride phase	83
23.	Samarium co-ordination in the fluorite lattice (four SmF_2 units)	85
24.	<pre>Sm(III) co-ordination a) Interstitial anion model</pre>	85 85
25.	Fluorite related rhombohedral unit cell	88

I. INTRODUCTION

The compound π -cyclopentadienylbis (acetylacetonato)-chlorozirconium(IV) presents an interesting opportunity to examine the properties of three classes of ligands: a monodentate chlorine, a bidentate acetylactonate, and a π -bonded cyclopentadienyl ligand. The preparation of this neutral complex, as well as the bromo- and benzoylacetonate analogs, was reported by Brainina and co-workers¹⁻³ who postulated an octahedral molecular configuration for these complexes, and noted the possibility of cis and trans isomerism. The infrared absorption spectrum was cited as support for a π -bonded cyclopentadienyl ligand and was not in conflict with octahedral stereochemistry.

An analogous compound, $\pi\text{-C}_5H_5(C_5H_7O_2)$ CrBr, has been prepared by Thomas⁴, who postulated an apparently tetrahedral molecular configuration. In both of these systems only one stereochemical site has been attributed to the cyclopentadienyl ligand, and the acetylacetonate ligand has been depicted in the <u>keto</u> rather than the <u>enol</u> form even though the latter would allow equivalent metal oxygen bond formation.

Considerable attention has been devoted to theoretical treatment of bonding between a central metal atom and a π -bonded cyclopentadienyl ligand. In a review of several of these calculations, Wilkinson and Cotton⁵ indicated the

probable formation of three low energy bonding molecular orbitals between the metal and the ligand. In an application of group theory to some mixed ligand cyclopentadienyl complexes, Cotton⁶ displayed molecular orbital diagrams (with estimated energy level separations) for (C5H5)NiNO and $(C_5H_5)Mn(CO)_3$. The cyclopentadienyl ligand portion of the diagram for the manganese complex is depicted with three low energy bonding molecular orbitals and three higher energy orbitals which may be described as nonbonding. The comparable diagram for the nickel complex displays the same general form but the energy level separation between the first and second bonding orbitals is considerably larger than that for the manganese complex. The stereochemistry of complexes containing cyclopentadienyl ligands has been discussed by assignment of three coordination sites to the ring⁷⁻⁹. If this interpretation is applied to the complexes reported by Brainina and co-workers¹⁻³ and Thomas⁴ their stereochemistry might be expected to reflect the geometry of six and eight coordination for chromium and zirconium respectively.

Several crystallographic investigations of acetylacetonate complexes have been compiled in a review by
Lingafelter and Braun¹⁰. These authors establish the equivalence of the C-O and C-CH bond distances as would be expected for the enol configuration of the ligand. Furthermore the ligand geometry appears to be essentially invarient with the exception of the O-O distance; this

distance and the OMO and MOC bond angles are determined by the particular metal atom and the stereochemistry of the complex.

The selection of $\pi \sim C_5H_5(C_5H_7O_2)_2$ ZrCl as the most suitable of the mixed ligand complexes was the result of several considerations. The four oxygen atoms from the acetylacetonate ligands and the chlorine atom represent five unambiguous stereochemical sites, as compared with only three in the $\pi \sim C_5H_5(C_5H_7O_2)$ CrBr complex. The rejection of the benzoylacetonate complex was a consequence of the packing requirements of the larger benzene ring relative to the smaller methyl group on the acetylacetonate and the desirability of the well characterized nature of this ligand. The chlorine derivative was selected in lieu of the bromine complex also as a result of packing considerations since the chlorine atom more closely approaches the size of the coordinate oxygen atoms.

Brainina and co-workers¹⁻³ have reported several preparative techniques for π -cyclopentadienylbis(acetylacetonato)-chlorozironium(IV). Preparation of the complex from $(\pi-C_5H_5)_2$ ZrCl₂ resulted in a 95% theoretical yield and the net reaction may be described by equation one:

$$(\pi - C_5H_5)_2ZrCl_2 + 2C_5H_8O_2 \longrightarrow$$

$$\pi - C_5H_5(C_5H_7O_2)_2ZrCl + C_5H_6 + HCl \qquad (1)$$

The $(\pi-C_5H_5)_2ZrCl_2$ was dissolved in a large excess of acetylacetone and maintained under reduced pressure at 70 to 80^0 for two hours. The volatile products, as well as about half

of the solvent, were distilled away as a result of the reduced pressure and the complex was obtained as a precipitate which was subsequently separated from the reaction mixture by filtration. The product was then washed with petroleum ether and dried, and the melting point determined both before and after recrystallization from benzene (188 - 190°). The compound was characterized by an elemental analysis, which agreed with the proposed composition, and by its infrared absorption spectrum.

Additional characterization of the complex has been reported by Pinnavaia et al. 11 These authors have investigated the solution behavior of the complex with conductance and proton nmr measurements. The conductance measurements, determined for a nitrobenzene solution, indicate a monomeric complex which is probably a weak electrolyte. Proton nmr spectra indicate the presence of non-equivalent environments for the methyl groups and -CH= protons on the chelate rings. Application of variable temperature nmr techniques is being pursued by these authors in an attempt to establish the existence of stereochemical isomers.

A structure determination of this complex has been effected by application of single crystal X-ray diffraction techniques in an attempt to clarify the stereochemical properties of the molecule.

The results of this investigation should be of value both for the prediction of probable stereochemical isomers of these molecules 11 and for interpretation of the geometry

of similar mixed ligand complexes, such as the complex ion $(\pi-C_5H_5)_2(C_5H_7O_2)$ Ti⁺ which has been prepared by Doyle and Tobias¹². They should also contribute to an understanding of the general chemistry of mixed ligand complexes containing one or more π -bonded cyclopentadienyl ligands.

II. EXPERIMENTAL

The preparation, represented by equation one, and characterization of the crystals of π -C₅H₅(C₅H₇O₂)₂ZrCl used in this investigation were effected by Dr. T. J. Pinnavaia of this department. The product had been recrystallized from dry benzene by allowing a saturated solution confined under a dry nitrogen atomsphere to cool slowly with stirring. Subsequent separation of the precipitate from the solvent was accomplished in the recrystallization vessel and the crystalline product was thoroughly dried in vacuo at 80° . An infrared absorption spectrum taken of the solid dispersed in a KBr matrix displayed no bands in the -OH stretch region (3400-3500 cm⁻¹); an indication that hydrolysis had not occurred. The observed melting point (189-1900) was in good agreement with that reported by Brainina et al. $(188-190^{\circ})$ and a carbon hydrogen analysis (found 46.0% C, 5.00% O; theoretical 46.2% C, 4.91% O; Galbraith Laboratories, Knoxville, Tenn.) was obtained to establish further the composition.

Crystal Properties

Crystals of the complex were examined with a Bausch and Lomb stereozoom variable power microscope and photographed with a Bausch

and Lomb Dynazoom metallograph. The hexagonal prismatic morphology of the transparent crystals, as displayed in Figure 1, is typical of their general form. The fairly soft crystals exhibited several cleavage planes, the sharpest of which was later determined to be nearly parallel to the (101) plane. A second cleavage plane, less sharply defined than the first was observed to be nearly parallel to the (011) plane. Several other cleavage planes, which could be reproduced only with difficulty, were not characterized.

An examination of the crystals with polarized light (Ernst Leitz Weltzer polarizing microscope) revealed distinct optical extinction axes (Figure 2), two of which were coincident with crystal faces, and a unique oblique extinction. These optical extinctions are indicative of a monoclinic unit cell and thus provided the first indication of the space group symmetry.

Characterization of the Unit Cell

The confirmation of the unit cell and the determination of the space group were accomplished by examination of precession and equi-inclination Weissenberg photographs taken with $CuK\alpha$ radiation.

Initial equi-inclination Weissenberg photographs obtained for a crystal rotating about the normal to the (110) plane displayed the characteristics of monoclinic symmetry and provided some of the criteria for the selection of the

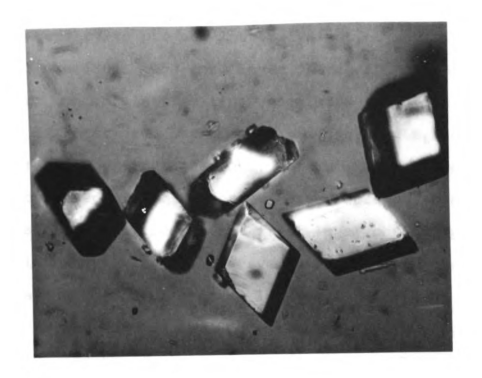


Figure 1. Crystals of π -C₅H₅(C₅H₇O₂)₂ZrCl.

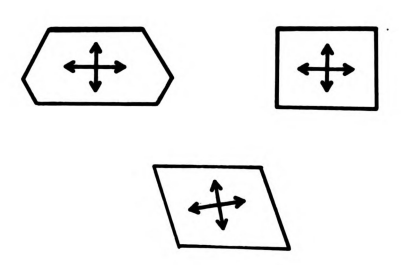


Figure 2. Optical extinctions.

space group. The angular repetition period, the angle of rotation necessary to produce the equivalent of any given reflection, was 1800. The zero layer photograph contained two distinct central lattice lines separated by 45 mm (90°) angle of rotation), one of which, designated B₁, displayed systematic extinctions (0k0, k = 2n + 1), and both of which possessed mirror symmetry. There were no observable central lattice lines on the first layer photograph, however, mirror symmetry was observable about an imaginary line overlaying the other central lattice line, A_1 , of the zero layer photograph. A curved festoon nearly overlaying B₁ was noted, and the festoons containing B₁ on the zero layer were overlayed by the equivalent set on the first layer. A central lattice layer line overlaying A₁ was observed on the second layer photograph (h0 ℓ extinct when ℓ = 2n + 1) while an additional shift was observed in the region of B₁. A subsequent precession photograph taken of the (101) reciprocal lattice plane confirmed the monoclinic unit cell.

Additional equi-inclination Weissenberg photographs were taken with a crystal rotating about the b-axis. The zero layer photograph contained a central lattice line, A_2 , which was identical to A_1 . The angle measured from the precession photograph (58°) and the separation displayed on a rotation photograph taken for the previous orientation facilitated selection of the remaining crystallographic axis. A comparison of the zero and first layer equi-inclination

photographs confirmed the hole extinctions described above while examination of additional layer photographs indicated no other apparent systematic extinctions. The observed systematic extinctions are uniquely described by the extinction requirements for the general positions of space group $P2_1/c$, which are displayed together with the general position coordinates in Table I. A schematic representation of the symmetry elements of the space group may be viewed in Figure 3.

Lattice Parameters and Density

Lattice parameters for monoclinic π -C₅H₅ (C₅H₇O₂)ZrCl were obtained from calibrated single crystal X-ray diffraction photographs taken with a Charles Supper non-integrating Weissenberg camera mounted on a Philips X-ray generator and exposed with $CuK\alpha$ radiation (40 kilovolts and 20 milliamperes). A goniometer head containing the single crystal used for intensity data collection (rotation about the b-axis) was mounted firmly on the camera. A single sheet of Ilford Industrial Type G X-ray film was encased in opaque paper and placed in the 57.3 mm diameter cassette. The cassette cradle on the Weissenberg camera was centered on the X-ray collimator, fixed rigidly in place, and the cassette placed on the cradle to its farthest extent. After a rotation photograph had been taken, the cassette and goniometer head were removed, and a second goniometer head containing an aligned recrystallized NaCl crystal was mounted firmly on

Table I. Properties of space group $P2_1/c$ (No. 14)

	Point Symmetry	Co-ordinates of Equivalent Positions	Conditions for Extinction
4 e	1	$x,y,z; \bar{x},\bar{y},\bar{z}; \\ \bar{x},1/2+y,1/2-z; x,1/2-y,1/2+z$	hk ℓ : no extinction ho ℓ : ℓ =2n + 1 Oko: k=2n + 1
2 d	ī	1/2,0,1/2; 1/2,1/2,0.	Fou 4-
2 c	ī	0,0,1/2; 0,1/2,0.	as for $4e$, plus hk ℓ :
2 b	ī	1/2,0,0; 1/2, 1/2, 1/2.	$k + \ell = 2n + 1$
2a	ī	0,0,0; 0,1/2,1/2.	

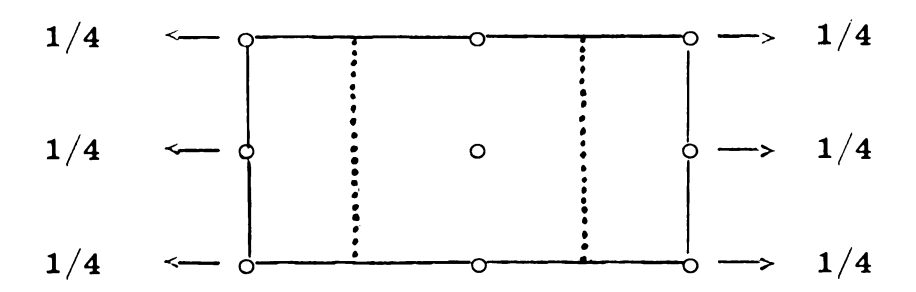


Figure 3. Representation of space group $P2_1/c$.

the camera after which the cassette was returned to its former position and a second rotation photograph was taken. An analogous procedure was followed to obtain a calibrated zero layer Weissenberg photograph for the same crystal orientation. The spot separation was determined to the nearest 0.01 mm with a Picker X-ray film reader, and correction factors were determined from a comparison of the observed NaCl lattice parameters with the known cubic value (a = $5.6387 \ \text{Å}$). The oblique monoclinic angle, β , was determined from the corrected a and c parameters and corrected dvalues obtained for holereflections. The lattice parameters, together with their standard deviations and expressed in coincidence with space group P2₁/c, are: a = 8.42 ± 0.01 , b = 15.66 ± 0.01 , c = $15.17 \pm 0.02 \ \text{Å}$, and $\beta = 123^025^{\circ} \pm 4^{\circ}$.

The density of π -C₅H₅ (C₅H₇O₂)₂ZrCl, as determined by the flotation technique with a solution of A.C.S. Reagent Grade carbon tetrachloride (ρ^{14} = 1.5863 g cm⁻³, 24°) and chloroform (ρ^{14} = 1.4816 g cm⁻³, 24°) employed as the immersion medium, was found to be 1.556 ± 0.005 g cm⁻³ at 24°. This value is in agreement with that calculated for the measured lattice parameters on the basis of four molecules per unit cell, 1.553 g cm⁻³.

Intensity Data Collection

Intensity data were collected with Ni filtered Cu radiation on a $0.12 \times 0.03 \times 0.07$ mm crystal by application of the multiple film equi-inclination Weissenberg technique.

A non-integrating Charles Supper Co. Weissenberg camera mounted on a General Electric X-ray generator equipped with a high intensity Cu tube was used to obtain data for levels hol through h8l ($\sin\theta/\lambda \leq 0.54$ Å Three sheets of Ilford Industrial Type G X-ray film were sandwiched between two pieces of opaque paper and placed in a cassette. Two twelve hour exposures (40 kilovolts at 38 milliamperes) were made for each layer; the first employed rotation from 0 to 190° and the second from 180 to 370°.

The film was processed by placing the exposed sheets in a light tight (5 x 7 in capacity) processing cassette and transferring this cassette to the appropriate solution tanks. All processing operations were carefully timed with a Gra Lab Universal Timer Model 168 viewed with the aid of a safe light used only after the film had been inserted into the processing cassette. The film was systematically agitated by raising and lowering the processing cassette at the following time intervals: development, every 30 seconds for five minutes; stop, every 15 seconds for one minute; and fix, every minute for fifteen minutes. The films were subsequently washed with a slow flow of distilled water for a minimum of one and one half hours, and allowed to dry thoroughly after which they were labeled and stored in clear cellophane envelopes.

An intensity calibration strip, for which two sheets of film were exposed, was prepared by incremented (\mathbf{I}_{n+1} = 1.15 \mathbf{I}_n) exposure of the (002) reflection. The relative

intensities were estimated visually by comparison of spots on the half of the film containing the reflections for which spot area is compacted with this calibration strip. An estimation of spot area as well as density was made and the intensities determined from each film were correlated and scaled to the inner-most film of the series. Scaling between adjacent sheets was accomplished by an increase of six in the calibration spot number obtained for the weaker film; this scale factor was determined from an examination of the two sheets of film exposed for the calibration strip and was found to account for changes in spot area as well as density. Reflections with an intensity less than the five cycle calibration spot were not recorded. Agreement between the estimated intensities from the first film and the scaled intensities was generally within 10% with apparently random deviations. A small number of reflections were duplicated on the two exposures made for each layer and agreement comparable with the inter-film estimated intensity deviation was obtained for these reflections. A total of 1453 different reflections (including the average intensity for duplicated reflections) from half the sphere of reflection was measured.

Absorption Correction

The linear absorption coefficient, μ = 74.7 cm⁻¹, for π -C₅H₅(C₅H₇O₂)₂ZrCl was calculated from tabulated¹⁵ mass absorption coefficients and the experimental density. The shape of the crystal used for the intensity data collection

and its orientation (a flat plate mounted with the rotation axis perpendicular to its broadest face) were such that application of the available absorption intensity correction program seemed desirable.

This program, written by Coppens, Leiserowitz, and Rabinovich¹⁶, is an extension of one written by Busing and Levy¹⁷. The correction factor, A = $\int (1/V) \exp[-\mu(r_i + r_d)] dV$ where V is the volume of the crystal, and r_i and r_d are the incident and diffracted beam path lengths, respectively, is evaluated numerically by the method of Gauss. The crystal, bounded by n plane surfaces, is described by a set of n inequalities which may be satisfied only if points which define the co-ordinate variables are inside of or on the surface of the crystal; these inequalities are used to determine the limits of integration necessary for the Gaussian approximation. As a consequence of this description of the crystal boundaries, no re-entrant angles between boundary planes may be included. These limits are used to establish a grid (dimensions m_x , m_y , and m_z) of points each of which is used to determine a value of r; and r_d . The net absorption correction for each reflection is determined as a weighted average over all points.

The crystal on which the intensity data were gathered was bounded by the eight plane surfaces tabulated in Table II, and was represented by a 16 x 6 x 10 (960 points) grid which resulted in the ratio $I_{cor}:I_{obs}=1.84\pm0.23$ (extreme values: 2.81 and 1.47).

Table II. Crystal boundary planes and their distance from the origin within the crystal.

		boundary nes	Distance from the origin (cm)
0	1	0	0.0022
0	1	0	0.0022
1	1	$ar{2}$	0.0034
1	1	2	0.0034
ī	1	$ar{2}$	0.0040
1	1	$ar{2}$	0.0040
1	0	0	0.0062
ī	0	0	0.0062

Computations

The calculations associated with the absorption correction described above and most of the remaining calculations were accomplished on a CDC-3600 computer (64K memory).

A number of programs, which had been either written or modified by Zalkin and obtained through his courtesy, were used throughout the solution of this structure. A description of the program used for intensity data reduction and Fourier's series calculations, as well as the full matrix least squares program used in this solution has been given by Shinn¹⁸. Intensity data, collected by equi-inclination Weissenberg techniques, are treated with two correction factors, the reciprocal of the Lorentz-polarization factor, $1/L-p = 2 \sin\theta \cos\theta/(1 + \cos^2\theta)$, and a velocity correction

factor $V = [1 - (h\lambda/2a\sin\theta)^2]^{1/2} / \sin\theta$ where a and h are the rotation axis parameter and the corresponding Miller index, respectively. The full matrix least squares program minimizes $\Sigma \ w(|F_0| - |F_C|)^2$ (w = weighting factor, F_0 and F_C are the observed and calculated structure factors, respectively), by varying the scale factor, x, y, z co-ordinates and, the thermal parameters, either isotropically or anisotropically. This program also calculates the standard deviations associated with the position co-ordinates and the thermal parameters. Distances and angles, with their standard deviations which result from the standard deviations of the position and lattice parameters, were calculated with program Distan described in Appendix I.

Planarity calculations were made with a program obtained from Dr. A. Tulinsky of this department. This program, which is also described in Appendix I, fits a least squares plane of the form AX + BY + CZ - D = 0 to a specified set of atoms and calculates the standard deviation of the plane, but does not include the standard deviations of either the position co-ordinates or the lattice parameters.

The stereographic projections of $\pi\text{-C}_5\text{H}_5\left(\text{C}_5\text{H}_7\text{O}_2\right)_2\text{ZrCl}$ and its unit cell were drawn on a CDC-6600 computer equipped with a cathode ray plotter with a program written by A. C. Larson.

III. STRUCTURE DETERMINATION

Patterson Synthesis

The Patterson function:

$$A_{(uvw)} = 1/v \sum_{h} \sum_{k} \sum_{\ell} |F_{hk\ell}|^2 \cos 2\pi (hw + kv + \ell w)$$

where $A_{(uvw)}$ is the peak height in terms of relative electron density at the ends of the real space vector u+v+w, v is the volume of the unit cell, and $v_{hk\ell}$ is the structure factor for reflection $v_{hk\ell}$, affords an opportunity to obtain valuable information from phase independent data and consequently represents the starting point for intensity data analysis in most crystallographic solutions.

This function exhibits certain symmetry relationships which are useful in the examination of a Patterson map (a two or three dimensional array of $A_{(uvw)}$ displayed as a function of u, v, and w). That the Patterson function (an even function) is centrosymmetric can be examined by considering two points A_1 and A_2 . The vector from A_1 to A_2 may be expressed as (uvw) while the vector from A_2 to A_1 would be $(\bar{u}\bar{v}\bar{w})$, and since any point in space may be viewed as the origin in a Patterson synthesis both of these vectors would be produced.

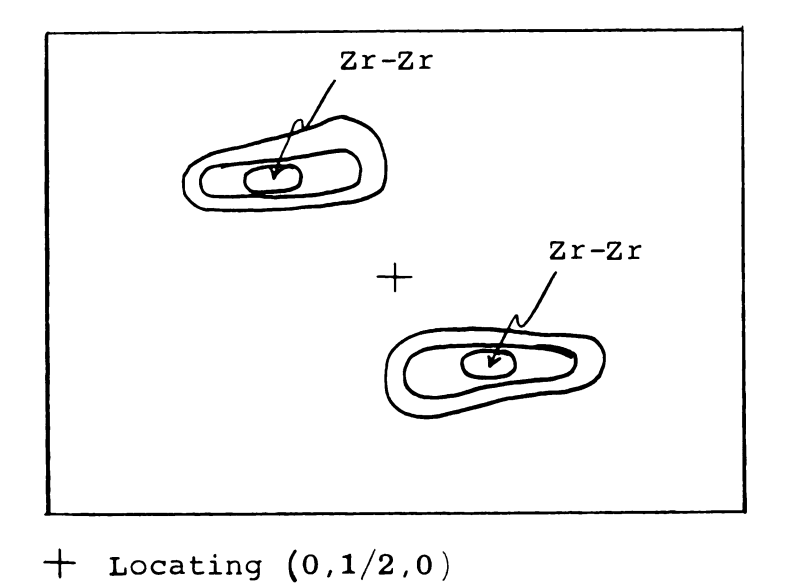
Consider now a diad screw axis parallel to the y-axis. This screw axis produces the following set of equivalent positions: x, y, z and -x, 1/2 + y, -z. A consideration of the three symmetry related points B_1 , (x_1, y_1, z_1) , B_2 , $(-x_1, 1/2 + y_1, -z_1)$, and B_3 , $(x_1, 1 + y_1, z_1)$, will illustrate a second symmetry property of the Patterson map. The vector from B_1 to B_2 may be expressed as (u,1/2,w) and similarly that from \mbox{B}_{2} to \mbox{B}_{3} as $(-\mbox{u},1/2\,,-\mbox{w})$. These vectors are related to each other by a simple diad axis. Thus any space group containing a two fold screw axis should produce vectors of the form (u, 1/2, w) in the Patterson map. Furthermore, these vectors are generated twice for every unique atom since the centrosymmetric nature of the Patterson synthesis generates the additional vectors (-u,-1/2,-w) and (u,-1/2,w) and the v=1/2 and v=-1/2 planes are coincident. It may also be shown in a similar manner that the vectors generated between two nonsymmetry related atoms of a space group with a two fold screw axis display the higher symmetry of a two fold axis through the origin of the Patterson map.

The investigation of one more important symmetry operation, the glide plane, remains. This plane produces the general transformation (with the glide taken in the direction of the c-axis) x,y,z to x,-y,1/2+z. If points C_1 , C_2 , and C_3 are generated as were B_1 , B_2 , and B_3 the points (x_1,y_1,z_1) , $(x_1,-y_1,1/2+z_1)$ and $(x_1,y_1,1+z_1)$ are produced for which the vectors between adjacent points are

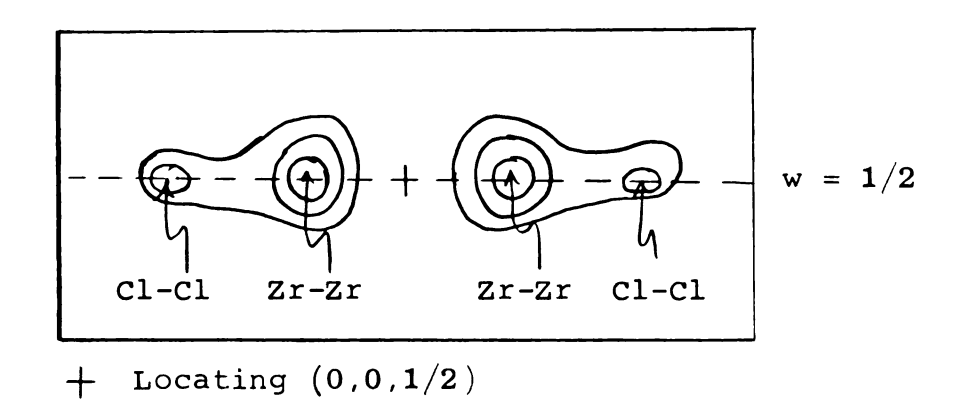
of the form (0,v,1/2). Application of the center of symmetry in the manner described above produces a second vector of this type. These coincident peaks are generally referred to as Harker peaks and are useful for determination of atomic co-ordinates. The set of vectors produced from non-symmetry related atoms in a unit cell containing a glide plane display mirror symmetry about the origin perpendicular to the y-axis.

The Patterson map for space group $P2_1/c$, which contains a center of symmetry, a diad screw axis parallel to the y-axis, and a glide plane with the glide direction along the z-axis and reflection perpendicular to the y-axis, should display a two fold axis parallel to and a mirror plane perpendicular to the y-axis. The symmetry of the Patterson map obtained for this solution may be viewed in Figures 4a and 4b.

The Patterson map for this space group should also contain Harker peaks of the form (u,1/2,w) and (0,v,1/2). The relationship between these Harker peaks and the atomic coordinates may be determined from the transformation equations of the space group: x,y,z; -x,-y,-z; -x,1/2 + y, 1/2 - z; and x,1/2 - y, 1/2 + z. The peak (u,1/2,w) may be shown to correspond to (-2x,1/2,1/2-2z) from which a solution for the x and z co-ordinates of the atom may be obtained. The second Harker peak (0,v,1/2) corresponds to $(0,1/2 \pm 2y,$ 1/2) and consequently may be solved for the y co-ordinate of the appropriate atom.



a) Symmetry of the $\mathtt{u},1/2,\mathtt{w}$ plane.



b) Symmetry of the (0,v,1/2) line.

Figure 4. Symmetry of the Patterson map.

As I have indicated, these peaks are generated twice for each unique atom in the unit cell and consequently have a peak intensity of twice that of the general vectors (u,v,w). Since every unique atom in the unit cell will produce a set of Harker peaks, their major application is found in the solution of crystal structures by the heavy atom technique. This structure investigation was well suited for solution by this technique. The ratio of $Z_{Zr}^2: \sum_i n_i z_i^2 = 1.45$ is nearly the generally accepted optimum value and thus calculations based on the phase contributions of the zirconium atom should produce a reasonably sensitive electron density map.

A Patterson summation, effected for half the unit cell with the absorption corrected data, produced the peaks and their corresponding co-ordinates displayed in Table III. Harker peaks corresponding to the zirconium atom were apparent and produced the co-ordinates: X=0.04, Y=0.160, and Z=0.140. Only the (0,v,1/2) Harker peak for the chlorine atom was included within the limits of the summation and was used to determine its Y co-ordinate. The remaining co-ordinates for the chlorine atom (X=0.300,Z=0.140) were determined by adding a general vector of the appropriate magnitude (2.52 Å) to the zirconium atom co-ordinates, and additional Zr-Cl peak assignments are contained in Table III.

Table III. Positions and intensities of principal Patterson peaks.

-x	Y	Z	Relative Intensity (999)
0.00	0.00	0.00	999
80.0	0.50	0.22	43 5 Zr-Zr
0.00	0.18	0.50	4 1 3 Zr-Zr
0.00	0.82	0.50	413 Zr-Zr
0.80	0.66	0.72	235 Zr-Zr
0.80	0.34	0.72	216 Zr-Zr
0.00	0.50	0.76	187 Zr <i>-</i> Zr
0.28	0.24	0.48	151 Zr-Cl
0.00	0.68	0.50	145 Cl-Cl
0.00	0.32	0.50	145 Cl-Cl
0.12	0.00	0.84	144
0.04	0.50	0.62	140
0.28	0.08	0.98	140 Zr-Cl
36	0.72	0.70	134 Zr-Cl
0.16	0.04	0.48	125
0.00	0.34	0.26	117 Zr-Zr
0.00	0.50	0.38	116
36	0.58	0.20	114 Zr-Cl
0.28	0.92	0.98	114 Zr-Cl
0.02	0.38	0.98	114
0.00	0.38	0.00	113
0.00	0.62	0.00	113
0.20	0.88	0.96	113
0.28	0.76	0.48	107 Zr-Cl
0.16	0.86	0.98	106
0.02	0.82	0.74	106
0.00	0.18	0.26	105
0.26	0.08	0.00	105 Zr-Cl

A subsequent least squares calculation with the atomic scattering factors for Zr and Cl calculated by Thomas and Umeda¹⁹ and Berghuis et al.²⁰, respectively, of these parameters produced the following values:

Light Atom Structure

The light atom structure was determined by application of the phase signs determined by the zirconium and chlorine atom positions in a Fourier's summation:

$$\rho_{(xyz)} = 1/V \sum_{h} \sum_{k} F_{hk\ell} \exp[-2\pi i(hx + ky + \ell z)], \text{ where}$$

 $ho_{(xyz)}$ is the electron density at point (xyz). The similar magnitudes of the atomic scattering factors for carbon and oxygen made assignment of their co-ordinates by peak height alone unreliable and consequently a three dimensional model of the electron density map was constructed. Subsequent comparison of the electron density model with the known geometrical configuration of the cyclopentadienyl and acetylacetonate ligands resulted in assignment of the peaks contained in Table IV.

A least squares calculation on these parameters with carbon and oxygen atomic scattering factors calculated by Berghuis et al. 20 produced R = 0.155.

Table IV. Electron density peak heights and assignments to atoms for π -C_5H_5(C_5H_7O_2)_2ZrCl

x	Y	Z	Peak Height	Atom
0.06	0.16	0.14	999	Zr
0.34	0.10	0.16	347	Cl
-0.34	-0.10	-0.16	347	Cl
0.18	0.28	-0.20	162	04
0.18	0.22	0.30	162	04
-0.18	0.28	0.08	138	01
0.18	0.28	0.12	136	03
-0.10	0.16	-0.04	128	02
-0.10	0.34	0.46	128	02
0.02	-0.02	-0.12	112	c_1^2
-0.02	0.02	0.12	112	c_1
0.22	0.34	0.16	107	C ₁₂
0.22	-0.04	-0.08	102	C_2
-0.22	0.04	0.08	102	C ₂
0.26	0.36	0.28	102	C ₁₃
0.06	0.50	0.38	99	C_1
0.06	0.02	0.24	94	C4
-0.26	0.28	-0.08	94	C 8
-0.26	0.22	0.42	94	C ₈
0.26	0.30	0.34	93	C ₁₄
0.26	0.20	-0.16	93	C ₁₄
-0.22	0.28	0.40	91	C ₇
-0.22	0.22	-0.10	91	C ₇
0.30	0.32	0.44	88	C_{15}
0.30	0.18	-0.06	88	$C_{1.5}^{1.5}$
-0.26	0.30	0.02	83	C _e
-0.06	0.08	0.26	83	C 4
0.22	-0.08	-0.16	79	C ₅
-0.22	0.08	0.16	79	C ₅
-0.26	0.20	0.50	7 5	C ₉
-0.10	0.50	0.26	73	C 4
0.26	0.44	0.12	73	C ₁₁
-0.26	-0.06	0.38	73	C_{11}
0.26	0.16	-0.20	71	C ₆
-0.26	0.30	0.30	69	C ₆
-0.26	0.20	0.20	69	C ₆
-0.02	0.46	-0.14	60	C ₁
-0.02	0.04	0.36	60	C ₁
-0.34	0.38	0.02	60	C_{10}
0.34	-0.10	0.48	58	C_{10}

Refinement of the Structure

The refinement proceeded in two phases: a) application of a weighting scheme and b) averaging of equivalent reflections.

Visual estimation of intensity data, accomplished as described previously, presents the probability of reading errors in addition to the errors associated with film collection of data. Reading errors would be expected to vary with both spot area and density and be of greatest magnitude for high intensity reflections. They would also be significant, particularly on a relative basis, for very weak spots. The intensity of very dense spots is determined by visual estimation of spot density on successive sheets of the multiple sheet film package exposed simultaneously and, with the exception of very strong reflection, may be averaged for two or more adjacent sheets of film. The intensity of weak reflections is obtainable from only the first sheet of film and thus may be averaged only by repeated reading of the same spot.

A weighting scheme is generally applied in order to let the most accurately obtained data have the greatest effect on the final refinement of the structure. This scheme should in some way represent the standard deviation in the data. Obtaining a direct estimate of the standard deviation of a series of reflections requires multiple determination of the intensity of each spot and is not practical for visual

estimation. The weighting schemes frequently applied to intensity data are those of Hughes 21 and Cruickshank which weight the data as the reciprocal of a function of $\left| \mathbf{F_0} \right|^2$.

A modification of these weighting schemes has been applied to the data in this solution. The modified scheme, the inverse of a parabola, is described by the following equation:

$$w = (A + |F_0|^2 - 2B|F_0| + B^2)/C)^{-1}$$

where A, B, and C are adjustable constants which determine the shape and minimum point of the parabola. A graphical display of this weighting scheme along with typical examples of the schemes of Hughes and Cruickshank may be examined in Figure 5. This scheme allows selection of a minimum value of $|F_0|$ which is believed to display favorable relative accuracy (A = 10 for this solution). Simultaneously it decreases the relative importance of weak reflections in the least squares refinement. This selection was made from an estimation of the intensity range most readily compared with the calibration strip (120 to 150 cycles for this investigation). The remaining constants, B and C, were determined by a trial and error procedure for which the minimization of R was the criterion.

An examination of $|F_0|$ and $|F_C|$ produced by a least squares treatment of the weighted data indicated random deviations for the intense reflections. Thus it would appear that the effects of extinction are smaller than the scatter in the estimated intensity data. The R factor

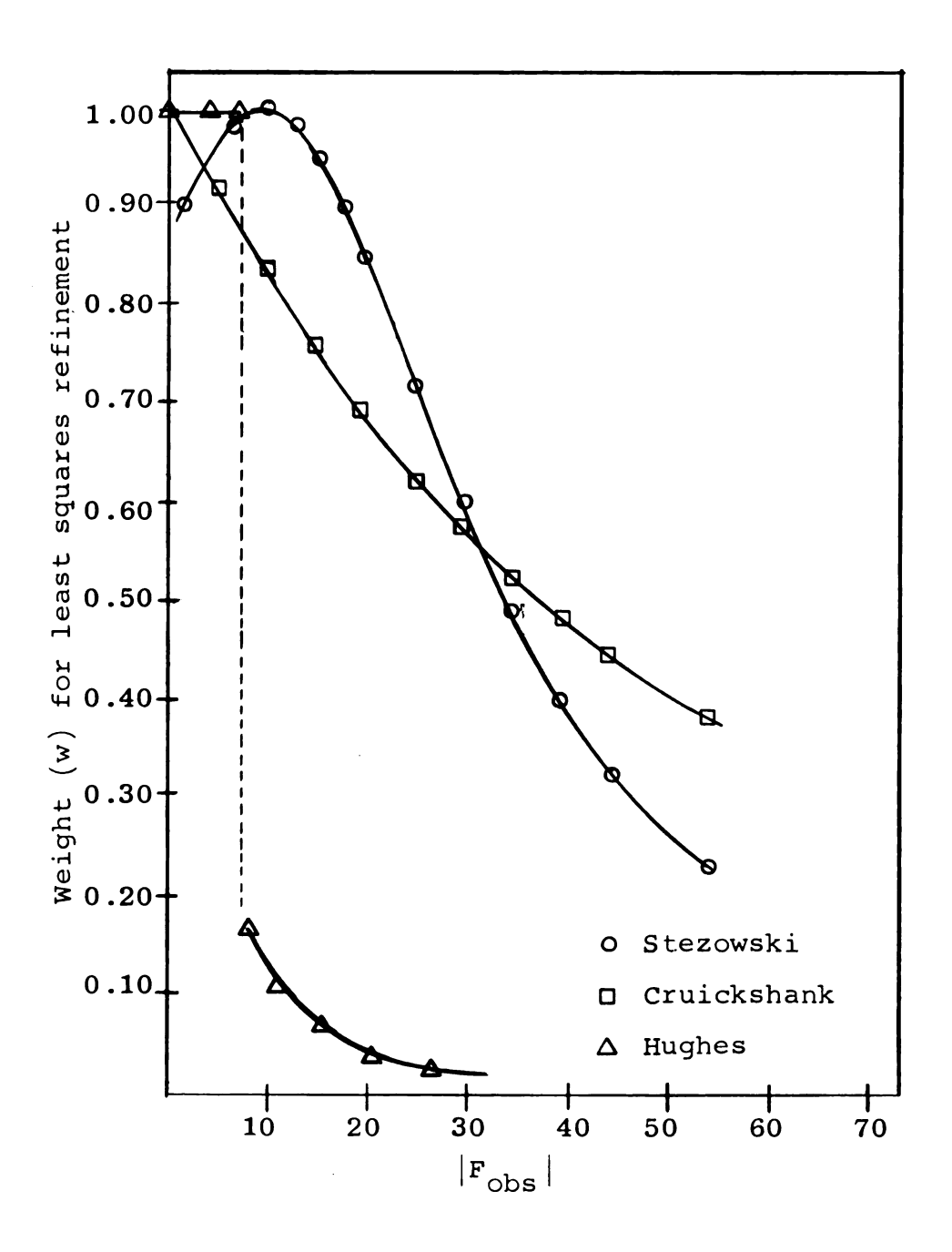


Figure 5. Comparison of weighting schemes.

obtained with the weighted data was 0.105.

Anamolous dispersion effects are significant for zir-conium when $CuK\alpha$ radiation is used (Table V), however, the centrosymmetric character of space group $P2_1/c$ and the optical activity of the molecule eliminate these effects.

The Laue symmetry, the symmetry of the intensity weighted reciprocal lattice, for monoclinic space groups is 2/m and results in the intensity relationship $\mathbf{I}_{hk\ell} = \mathbf{I}_{\bar{h}k\bar{\ell}}$. The intensity data set for this solution was collected over half the sphere of reflection and contained a number of equivalent reflections of this type. A portion of these reflections, $\mathbf{I}_{\bar{h}k\ell} = \mathbf{I}_{hk\bar{\ell}}$ (only this symmetry requirement was initially recognized) were averaged in an effort to reduce the effects of random errors and this reduced data set was employed for the final refinement.

Table V. Dispersion corrections for zirconium.

	$f = f_0 + \Delta f' + i\Delta f''$	
Sin θ/λ	Δf'	Δ f"
0.0	-0.6	2.5
0.6	-0.7	2.2

The parameters which had been obtained from least squares refinement with the entire data set were subjected to further

refinement by least squares treatment with the 1131 reflections. The refinement was continued (no zero weighted data) with isotropic thermal factors until the shift in all the parameters was less than 0.001 times their respective standard deviations. This refinement was effected with the atomic scattering factors for Zr, Cl, O, and C reported by Cromer and Waber²³, and produced a final R factor of 0.093. The parameters obtained from the final isotropic least squares refinement, with their standard deviations are displayed in Table VI, and the calculated and observed structure factors for each reflection are presented in Table VII.

A subsequent refinement of the parameters with anisotropic temperature factors for all atoms (no special positions) produced an R of 0.083. This small change in R compared to the isotropic case would appear to reflect fairly high random deviations in the intensity data and consequently all subsequent calculations were based on the parameters obtained from the isotropic refinement. The atomic co-ordinates and the anisotropic thermal parameters are tabulated in Appendix II.

Table VI. Atomic co-ordinates for $\pi\text{-C}_5\text{H}_5\left(\text{C}_5\text{H}_7\text{O}_2\right)_2\text{ZrCl}$.

Atom	Symbol in Figures	х	Y	Z	В
Zr Cl	Z P	0.0439(3)* 0.3356(9)	0.1657(2) 0.1006(5)	0.1414(2) 0.1655(5)	4.23 (.07)**5.20 (.16)
Cyclo	opentadi	enyl ligand			
C ₁ C ₂ C ₃ C ₄ C ₅	C C	-0.0550(39) -0.2174(36) -0.2217(40) -0.0421(36) 0.0660(35)	0.0038(19) 0.0534(19) 0.0997(20) 0.0837(10) 0.0298(20)	0.1186(22) 0.0761(20) 0.1525(22) 0.2541(20) 0.2331(20)	6.49 (.66) 5.30 (.59) 6.19 (.65) 5.59 (.62) 5.47 (.58)
Acety	ylaceton	ate ligands			
O ₁ O ₂ C ₆ C ₇ C ₈ C ₉ C ₁₀	O A A A	-0.1708(20) -0.0901(20) -0.2580(32) -0.2108(33) -0.2920(34) -0.2694(31) -0.3694(38)	0.2661(11) 0.1614(12) 0.1918(17) 0.2196(18) 0.2880(17) 0.3082(17) 0.3895(20)	0.0950(12) -0.0238(11) -0.1073(18) -0.0982(19) -0.0858(20) 0.0074(18) 0.0151(22)	4.40 (.33) 4.44 (.31) 4.86 (.52) 4.65 (.54) 4.15 (.56) 5.15 (.50) 6.50 (.67)
0 ₃ 0 ₄ C ₁₁ C ₁₂ C ₁₃ C ₁₄ C ₁₅	N N B B B	0.1680(20) 0.1867(21) 0.2526(38) 0.2238(31) 0.2659(33) 0.2510(32) 0.3072(31)	0.2782(12) 0.2232(13) 0.4264(20) 0.3497(18) 0.3638(17) 0.3027(19) 0.3167(18)	0.1193(12) 0.2928(12) 0.1173(22) 0.1685(17) 0.2682(19) 0.3267(18) 0.4386(17)	4.86 (.35) 4.82 (.35) 6.52 (.67) 4.36 (.49) 4.60 (.55) 4.44 (.52) 4.99 (.54)

Numbers enclosed by parentheses are standard deviations multiplied by $10^4\,\cdot$

^{**}Standard deviations

Table VII. Observed and calculated structure factors.

	1 118 227 - 37 8 37 8 37 8 - 2 8 7 10 38 38 3 10 98 - 37 10 38 3 10 98
--	--

IV. DESCRIPTION OF THE STRUCTURE

The Unit Cell

The arrangement of the atoms and molecules in the unit cell may be examined in three dimensional stereo by viewing Figures 6 and 7 with a standard stereoscope. The correlation of the symbols in these Figures with the atoms in the molecule has been presented in Table VI. The symbols representing the atoms contained within individual ligands are connected with solid lines while the co-ordinate atoms, with the exception of the carbon atoms of the cyclopentadienyl ligand, are connected to the zirconium atom with dotted lines. The proximity of the cyclopentadienyl ligand to a single zirconium atom establishes the molecular unit.

A layer structure, consisting of molecular units arranged nearly parallel to the yz plane, a cleavage plane, may be ascertained from Figure 6. The molecular packing of these layers exhibits several interesting properties. An internal fold of $15.6 \pm 0.03^{\circ}$ between the plane described by the O-Zr-O segment and the acetylacetonate ligand (standard deviation of the ligand planes $\sigma = \pm 0.05 \ \text{Å}$) draws the ligands closer together and thus favors formation of the distinct layers. This flexibility of an acetylacetonatemetal bond has been observed in

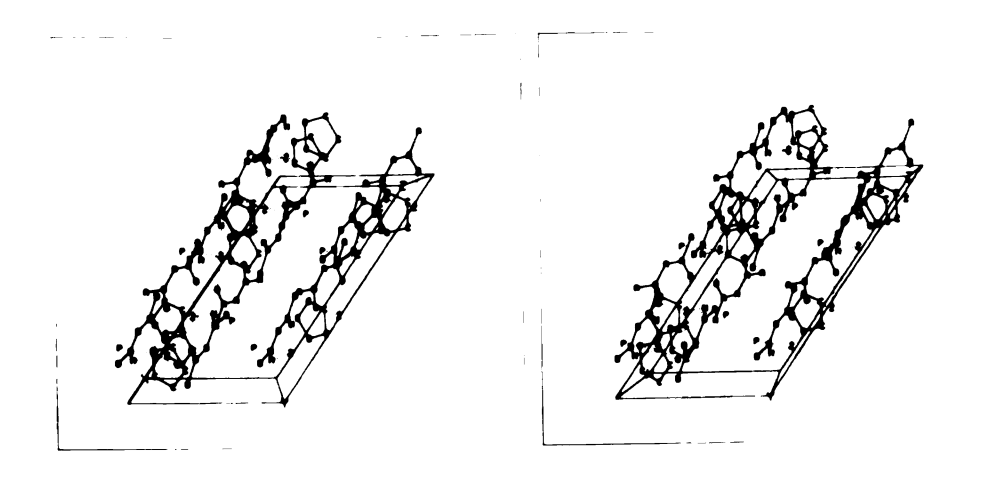


Figure 6. Stereographic projection of the unit cell.

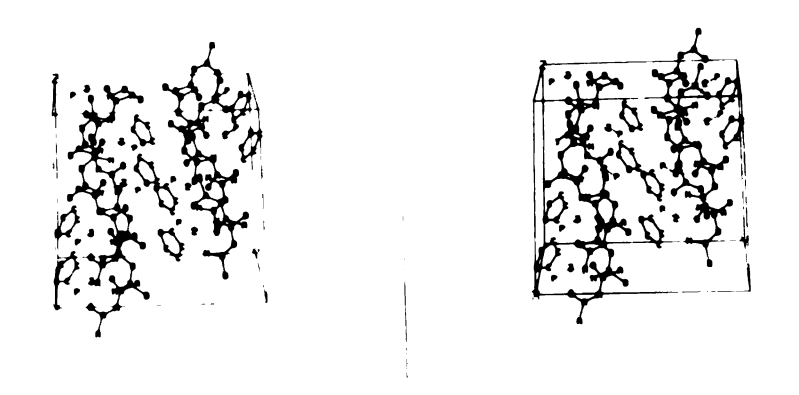


Figure 7. Stereographic projection of the unit cell.

tetrakisacetylacetonatozirconium(IV) for which Silverton and Hoard²⁴ report a mean fold angle of 22.6°.

The orientation of the cyclopentadienyl ligand with respect to adjacent molecules is also of interest. adjacent molecules, which are related by a center of symmetry, display an interesting intermolecular arrangement of the cyclopentadienyl ligand with respect to an oxygen atom (symbol 0). One cyclopentadienyl carbon atom is directed toward an oxygen atom in a manner compatible with hydrogen bonding and the center of symmetry between these molecules results in a second such orientation between the same two molecules. However, the likelihood of hydrogen bonding between these atoms may be discounted for two reasons: a) the ligand is basic in character since one hydrogen has been removed in the formation of the complex and b) the distance between the oxygen and the carbon atoms is 3.49 \pm 0.03 Å, slightly greater than the sum of the van der Waals radii²⁵ for a methyl group and an oxygen atom (3.40 Å).

The basic character of the cyclopentadienyl ligand raises the possibility of hydrogen bonding between the electron cloud above the ring (away from the Zr atom) and an acidic hydrogen atom. Examination of Figures 6 and 7 fails to produce any favorable geometrical arrangement with respect to the ligand plane and consequently this type of hydrogen bonding appears unlikely. Another potential site for hydrogen bonding, also basic in character, is the chlorine atom. The possibility of interlayer interactions

seems geometrically feasible for the hydrogen atom on the gamma carbon atom of both acetylacetonate ligands of one molecule with the same chlorine atom in an adjacent layer. The same criteria that made the formation of $C-H\cdot O$ hydrogen bonds unlikely apply to the formation of these $C-H\cdot Cl$ bonds. The gamma carbon atom lost one hydrogen atom in the formation of the complex and thus should be basic rather than acidic. Furthermore the nearest approach between the relative atoms is 3.76 ± 0.03 Å, a value equal to the sum of the van der Waals radii²⁵ for a chlorine atom and a methyl group. Since formation of hydrogen bonding appears unlikely, interlayer and intermolecular attractions are confined to the interaction of van der Waals forces. This hypothesis is supported by the soft texture of the crystals.

The staggered arrangement of the cyclopentadienyl ligands displayed in Figure 7 produces an irregular layer structure nearly parallel to the xz plane of the unit cell. These layers appear coincident with the less consistent cleavage plane observed for this orientation of the crystal. Less obvious planar relationships may be noted to crisscross the unit cell in a manner that produces somewhat irregular layers one molecule thick, and account for the large number of cleavage planes infrequently observed when several crystals were cleaved in varying directions.

Packing considerations do not appear to have seriously affected the positions of the coordinate atoms and consequently the stereochemistry of the molecule should reflect

the effects of the bonding between the zirconium atom and the ligands. Neither do these constraints appear to have operated on the O-O separation of the acetylacetonate ligands, nor to have significantly affected the incline of the cyclopentadienyl ligand with respect to the rest of the molecule.

Molecular Geometry

The molecular geometry of π -C₅H₅(C₅H₇O₂)₂ZrCl is displayed as a stereographic projection in Figure 8. The spheres that enclose the symbols represent the magnitude of the isotropic thermal parameters (Table VI). The fold in the two acetylacetonate ligands may be noted in this figure as well as in Figures 6 and 7. This fold is away from the cyclopentadienyl ligand for one acetylacetonate ligand and away from the chlorine atom for the other. It appears to result from packing in the unit cell rather than repulsion between the appropriate ligands, since carbon atoms of the acetylacetonate ligand closest to the cyclopentadienyl ring are at distances greater than 4 Å from it, and similarly carbon atoms of the other acetylacetonate ligand are more than 4 Å from the chlorine atom.

The molecule, which displays only C_1 symmetry, may be described as the <u>cis</u> configuration of an octahedron in the manner proposed by Brainina <u>et al.</u>¹. The three oxygen atoms and one chlorine atom (0,0,N, and P, in Figure 8) may be considered to constitute the four co-ordinate plane

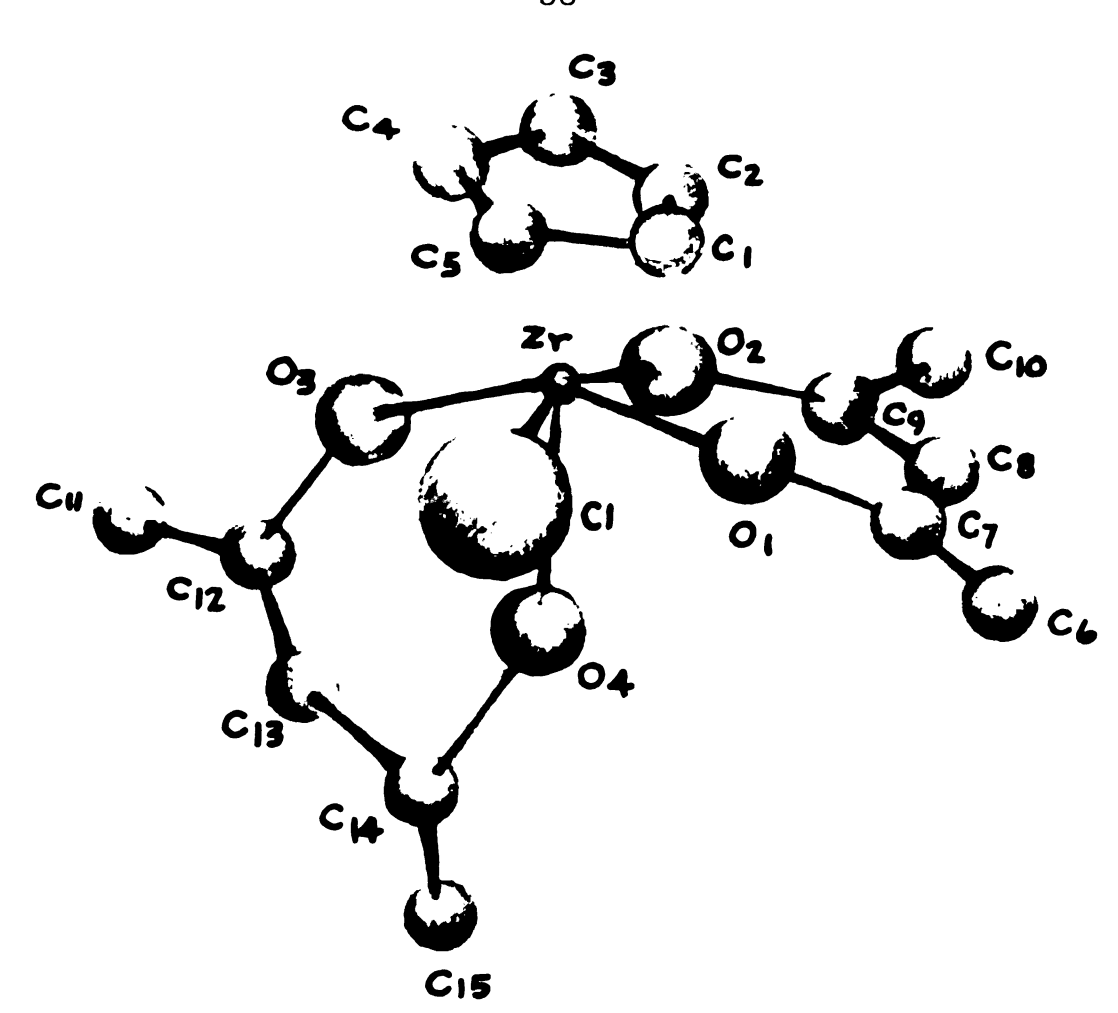




Figure 8. Projections of the molecule.

of the octahedron. The least squares plane fitted to these atoms was found to have a standard deviation of 0.06Å. The two remaining octahedral sites would be occupied by the cyclopentadienyl ligand (C) and the remaining oxygen atom (N). The least squares plane containing the cyclopentadienyl ligand, standard deviation 0.03 Å, is nearly parallel to the four co-ordinate plane; the angle of intersection between these planes is 3.0° . A significant deviation from the octahedral geometry occurs for the zirconium atom position, which is 0.45 Å out of the four co-ordinate plane.

Selected interatomic bond distances and angles are displayed in Table VIII. The cyclopentadienyl ligand planarity and the average bond length, together with the average bond angle are in agreement with the theoretical values calculated for a ring with five equivalent bonds. The one unusually long C-C bond distance, 1.51 Å, spans the chlorine atom site and probably results from packing effects.

A comparison of the bond lengths and angles for the acetylacetonate ligands with comparable parameters for octahedral transition metal complexes (Table IX) is of interest. Although there is general agreement, the OMO bond angle (79.1 \pm 1.3°, average deviation) and the mean C-O bond length (1.32 \pm 0.04 Å) for this complex differ markedly from the mean values for the octahedral complexes (93.2 \pm 4.7° and 1.27 \pm 0.02 Å, respectively). The mean OZrO bond angle for this structure compares more favorably with that reported for the eight co-ordinate ${\rm Zr}({\rm C_5H_7O_2})_4^{24}$ (75.0 \pm 0.2°).

Table VIII. Selected interatomic bond lengths and angles

· ·	1-Atom(s)	Dist O A	Atom 1	Atom 2	Atom 3	Angle deg
Cyclo	pentadienyl	Ligand:				
$\mathtt{C_1}$	\mathtt{C}_{2}	1.38(3)*	C ₅	$\mathtt{C_1}$	\mathtt{C}_{2}	104.3(2.0)*
C_2	·. С ₃	1.39(3)	$\mathtt{C_1}$	C_2	C ₃	112.3(2.0)
C3	C ₄	1.46(3)	\mathtt{C}_{2}	C ₃	C_4	107.7(2.0)
C_4	C ₅	1.40(3)	C ₃	C ₄	C 5	107.0(1.9)
C ₅	C_1	1.51(3)	C_4	C ₅	C_1	108.1(1.8)
Avera	ge C-C	1.43(5)				107.9(2.9)
Avera	ge Zr-C	2.55(5)				
Acety	lacetonate	Ligands:				
Zr	01	2.20(1)	01	Zr	02	80.4(0.5)
Zr	02	2.11(1)	$C_{f 4}$	01	Zr	129.9(1.2)
01	02	2.78(2)	\mathtt{C}_{2}	02	Zr	129.3(1.2)
01	C ₄	1.30(2)	01	C_{4}	C ₃	126.3(2.0)
02	\mathtt{C}_{2}	1.36(2)	02	C_2	C_3	127.5(1.7)
C ₃	C ₄	1.36(3)	C_{4}	C ₃	C_2	123.8(1.9)
C_2	C ₃	1.34(3)	C ₅	C_4	01	113.0(1.7)
C_4	C ₅	1.56(3)	C_1	$\mathtt{C_2}$	\mathtt{O}_{2}	109.9(1.7)
C_1	\mathtt{C}_{2}	1.53(3)				
Zr	03	2.16(2)	0 3	Zr	04	77.8(0.5)
Zr	04	2.13(1)	C ₇	03	Zr	132.2(1.1)
03	04	2.69(2)	C ₉	04	Zr	132.4(1.2)
03	C ₇	1.30(3)	03	C ₇	C ₈	125.0(2.0)
04	C ₉	1.33(3)	04	C ₉	C ₈	125.5(1.8)
C7	C ₈	1.38(3)	C ₇	C ₈	C ₉	122.5(2.1)
C ₈	C ₉	1.35(3)	C ₆	C7	03	120.1(1.7)
C ₉	C ₁₀	1.52(3)	C ₁₀	C ₉	04	111.8(1.8)
C ₆	C ₇	1.51(3)				
Zr-C	1	2.50(1)				

Zr-Cyclopentadienyl ligand plane = 2.24(2)

 $^{^{\}ast}$ The values listed in parentheses are the standard deviations of the last digit(s).

The Zr-O mean bond length obtained in this solution (2.15 \pm 0.04 $\mbox{\ensuremath{\upalpha}}$) is also in reasonable agreement with those reported for $Zr(C_5H_7O_2)_4$ (2.198 \pm 0.009 $\mbox{\ensuremath{\upalpha}}$) and for the $Zr(C_2O_4)_4^{4-}$ complex ion²⁵ (2.199 \pm 0.009 $\mbox{\ensuremath{\upalpha}}$). In addition, the intraligand O-O separation (2.73 \pm 0.04 $\mbox{\ensuremath{\upalpha}}$) falls midway between the mean value reported for tetrakisacetylacetonatozirconium(IV) (2.67 $\mbox{\ensuremath{\upalpha}}$) and that for the octahedral complexes (2.80 $\mbox{\ensuremath{\upalpha}}$).

Table IX. Summary of interatomic parameters for some hexaco-ordinate transition metal* acetylacetonate complexes.

Atom	1-Atom(s) 2	Dist A	Atom 1	Atom 2	Group 3	Angle deg
0	О	2.80(4)**	÷ 0	M	0	93.2(4.7)
С	О	1.27(2)	M	0	С	125.3(3.3)
С	СН	1.38(2)	0	С	СН	125.6(1.4)
С	CH ₃	1.53(3)	0	C	CH ₃	124.4(2.8)
			С	СН	С	114.0(1.2)

Metals considered are Mn, Cr, Co, and Fe.

Adapted from Lingafelter and Braun 10

Zirconium compounds demonstrate a marked tendency to adopt lattice arrangements that produce stereochemical configurations which are related to the geometry of eight coordination. A number of these compounds have been tabulated by Nyholm et al. 9 For example, the ${\rm ZrF_4}$ lattice 27 is arranged in a square antiprismatic configuration and the ${\rm ZrF_6}^{2-}$ ion 28 has been found to crystallize as a chain-like

The values contained in the parentheses are the standard deviations in the last digit for the averaged values.

polymer with dodecahedral links, while the $Zr(C_5H_7O_2)_4$ and $Zr(C_2O_4)_4^{4-}$ complexes are examples of discrete square antiprismatic and dodecahedral arrangements, respectively.

In an analysis of eight co-ordination Hoard and Silverton²⁹ discuss three configurations of possible stereochemical merit: the square antiprism, the undecahedron, and the dodecahedron. The undecahedron has not been reported as a suitable model for any discrete eight co-ordinate species, but has been invoked by Zachariasen to explain the co-ordination of Th₇S₁₂³⁰ and PuBr₃³¹, and several compounds isostructural with PuBr₃ have been tabulated by Nyholm et al.⁹ The equations for the dodecahedral and square antiprismatic valence bond orbitals have been proposed by Duffey³², ³³ and Racah³⁴, and extensive calculations for the ligand-ligand repulsion energies for these models have been reported both by Kepert³⁵ and by Parish and Perkins³⁶.

The presence of different ligands in π -C₅H₅(C₅H₇O₂)₂ZrCl eliminates the possibility for a close approximation to the symmetry of any of the ideal stereochemical models and therefore reduces application of a model to a general description of the overall geometry of the complex. The ambiguity associated with the co-ordination of the cyclopentadienyl ligand further confines application of the model to a description of the orientation of the plane of this ligand rather than the designation of positions for specific carbon atoms. Schematic representations of the square antiprism (Figure 9), the undecahedron (Figure 10), and the dodecahedron (Figure 11)

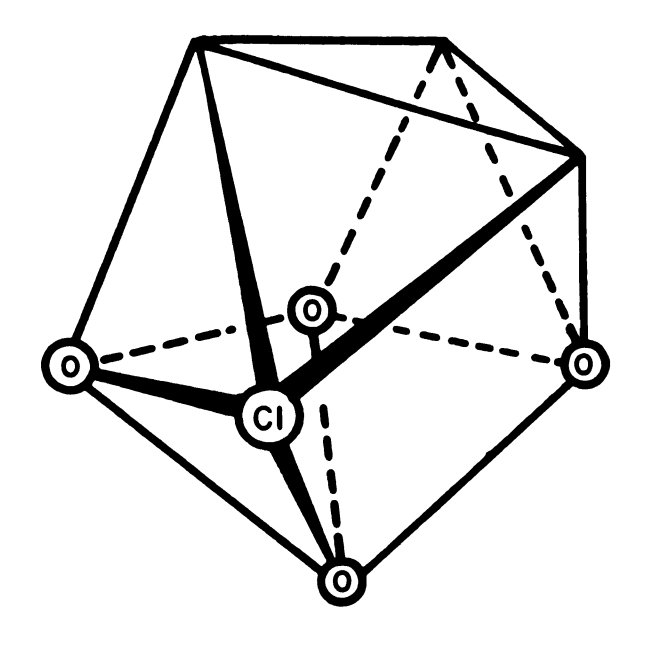


Figure 9. Square antiprism.

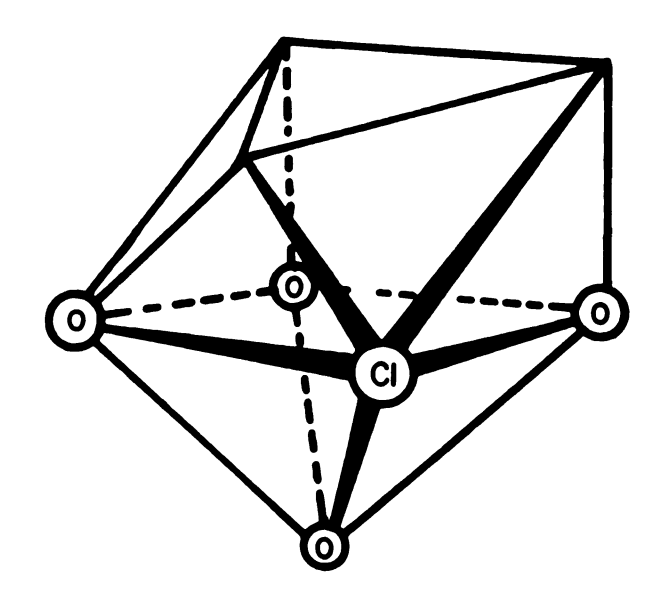


Figure 10. Undecahedron.

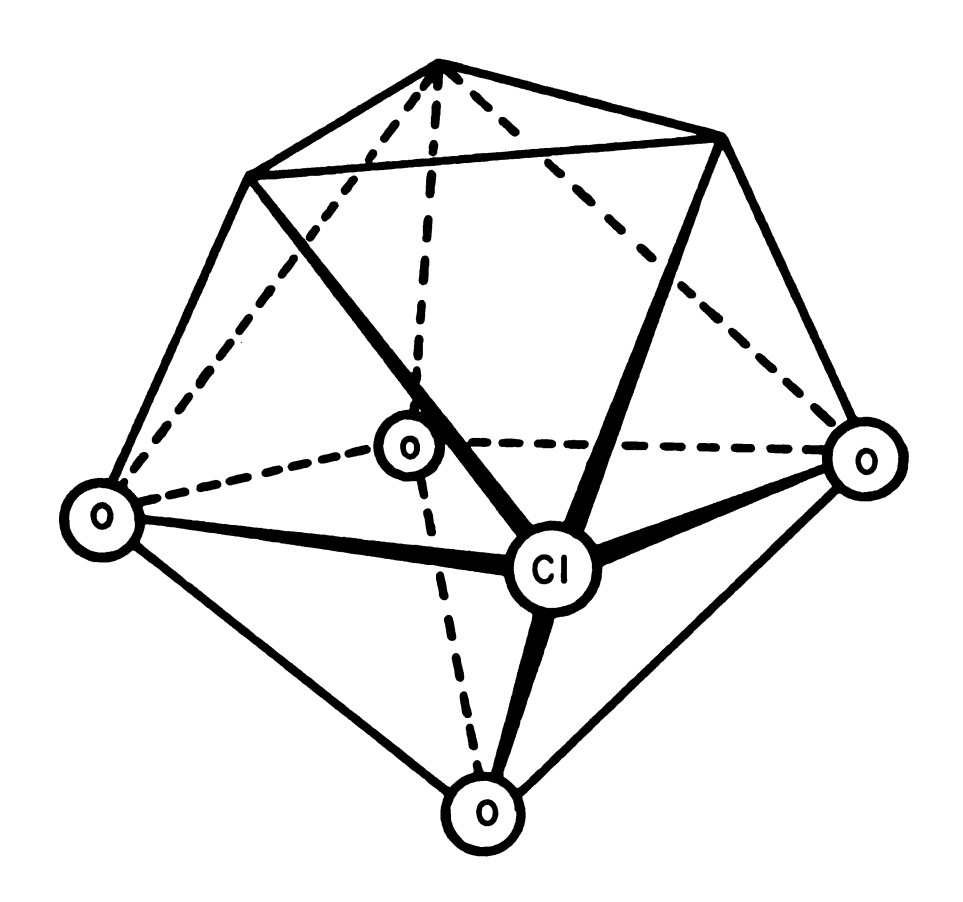


Figure 11. Dodecahedron

have been constructed with the positions of the chlorine and oxygen atoms chosen to most closely approximate the geometry of the molecule.

On the basis of ligand-ligand repulsion calculations the most stable configuration for eight co-ordination is the square antiprism (approximately 1 kcal/mole more stable than the dodecahedron)³⁶. The symmetry of the ideal square antiprism (D_{4d} - $\overline{8}2m$) gives rise to two sets of eight symmetry related edges designated ℓ and s by Hoard and Silverton²⁹. The ratio of the ℓ and s edges for a number of zirconium complexes¹⁸,³³,³⁴ averages to 1.05, and θ , the angle between the $\overline{8}$ axis and a co-ordinate bond, is approximately 57.5°. An examination of Figure 9 indicates the lack of compatibility of this model with the geometry of π - $C_5H_5(C_5H_7O_2)_2ZrCl$. One O-Cl distance would have to be approximately $\sqrt{2}$ times the other (observed ratio 0.95) and the angle 2θ , ClZrO, is 90.2 \pm 0.3° and not 115°.

There is considerable merit for consideration of the undecahedron $(c_{2V}^{}-mm^2)$ as a model for this compound. For example, if a special case of this model is considered it closely resembles an octahedron with the zirconium displaced from the four co-ordinate plane. A mirror symmetry plane perpendicular to the four co-ordinate plane requires opposite edges of this plane to be equal. This model may be considered the equivalent of an octahedron if all four sides are equal; an acceptable condition for this structure, if the larger size of the chlorine atom relative to the oxygen

atom is taken into consideration. Placement of the zirconium atom on the mirror plane and on the two fold axis (at the origin of the polyhedron) displaces it from the four co-ordinate plane. The resultant orientation of the cyclopentadienyl ring with respect to the four co-ordinate plane is also compatible with the observed structure.

If the molecule is describable in terms of the octahedral case of the undecahedral model the angles formed by the four co-ordinate positions and an origin defined by projecting the zirconium atom onto the plane should be right angles (Figure 12) or for the more general case the adjacent angles should be supplementary (Figure 13). The extension of one corner due to the larger size of the chlorine atom would not effect these angles beyond the possible packing effects. The appropriate angles are displayed in Figure 14 and clearly do not fit either criterion for this model. They do, however, more closely approximate the expected results for a similar operation carried out for dodecahedral symmetry (Figure 15).

The dodecahedral polyhedron contains two sets of symmetry related positions which may be designated as the A and B sites in the manner of Hoard and Silverton²⁹. This configuration may be constructed for this mixed ligand molecule by placing the chlorine atom and one oxygen atom from each acetylacetonate ligand in B positions and the remaining oxygen atoms in A positions (Figure 11). The observed oxygen-chlorine plane consists of an A and three

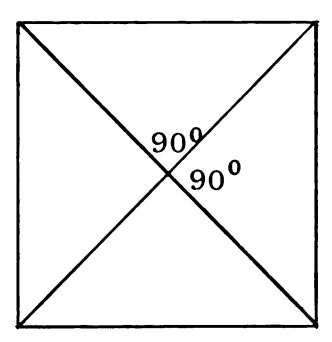


Figure 12. Projected co-ordinate angles for the octhedral undecahedron.

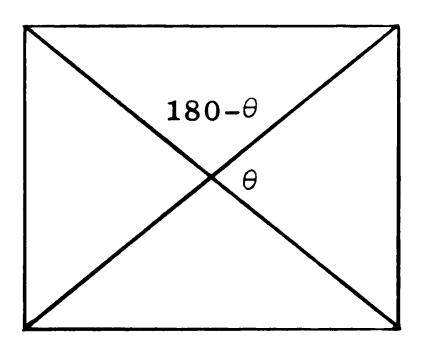


Figure 13. Projected coordinate angles for the general undecahedron.

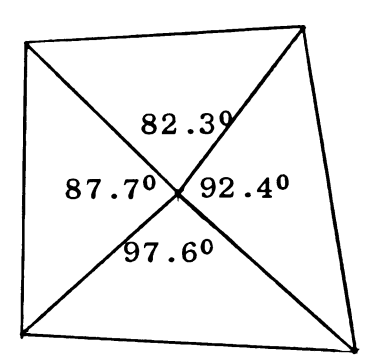


Figure 14. Projected co-ordinate angles for the $\pi-C_5H_5\left(C_5H_7O_2\right)_2$ ZrCl.

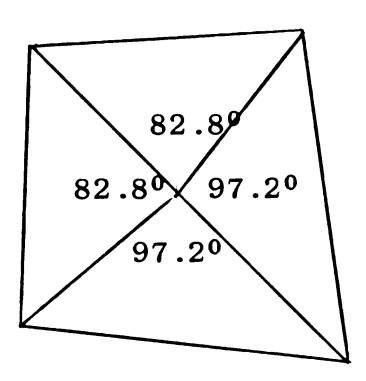


Figure 15. Projected coordinate angles for the dodecahedron

B sites, in which case centering the zirconium atom on the S_4 axis of an ideal dodecahedron results in its displacement above this plane in the manner observed.

Dodecahedral molecular geometry is generally characterized by two sets of angles, $\theta_{\mathbf{A}}$ and $\theta_{\mathbf{B}}$, and the ratio of the bond lengths. Appropriate parameters for this molecule are: $\theta_{A} = 37.8^{\circ}$ (no meaningful deviation, only one measurement), $\theta_{\rm B} = 77.8 \pm 0.3^{\circ}$, ${\rm Zr-O_{\rm A}} : {\rm Zr-O_{\rm B}} = 1.03 \pm 0.02$. Similar parameters calculated by Silverton and Hoard²⁴ for the ideal D_{2d}^{-42m} model ($\theta_A = 35.2^{\circ}$, $\theta_B = 73.5^{\circ}$, M-A:M-B = 1.03) and for a hard sphere model ($\theta_{\rm h}$ = 36.90, $\theta_{\rm R}$ = 69.50, M-A:M-B = 1.00) are in reasonable agreement with the values observed for this structure. Additional characterization of a dodecahedron is obtained from a comparison of the four symmetry related edge lengths, or more appropriately, their ratios. The values for this structure (m/a = 1.03, g/a =1.05, and b/a = 1.25) may be compared with the analogous ratios for both the D_{2d} - $\overline{4}2m$ (m/a = 1.00, g/a = 1.06, and b/a = 1.27) and the hard sphere models (m/a = g/a = 1.00, and b/a = 1.25). The large m/a ratio found for this molecule arises from the larger size of the chlorine atom which occupies one of the sites determining the only unambiguous edge.

As a further check on the dodecahedral molecular configuration a series of calculations were made based on the θ_A and θ_B angles of the $D_{2d}^{-4}2m$ dodecahedron and the mean bond distance for the observed Zr-O bonds (2.15 Å).

The co-ordinates of three B and four A positions were generated by defining the z axis coincident with the S4 axis of the dodecahedron and by assigning the first A and B sites to the xz and yz planes, respectively, and operating on them with the S_4 symmetry operations. The remaining site was determined by extending the fourth B site, generated from the above operations, to a length of 2.50 Å (the Zr-Cl bond length). Calculations based on this model produced a four co-ordinate least squares plane (one A and three B sites, $\sigma = \pm 0.04 \text{ Å}$), which is comparable to the oxygen-chlorine plane of the observed molecule, and indicated that the origin (zirconium) was 0.64 Å from this plane. Similar calculations on three of the remaining dodecahedral sites, which may be assigned to the cyclopentadienyl ligand, established a 5.40 angle of intersection between the two planes. For this complex the standard deviation of the oxygen-chlorine plane is \pm 0.06 $\overset{\circ}{A}$, and the angle of intersection between the cyclopentadienyl ligand and the four co-ordinate plane is 3.00. The agreement between the observed structure and this model is considered reasonably good since distortion due to both repulsion and packing effects was not considered. It must be emphasized that the use of the three co-ordination sites for the cyclopentadienyl ligand in no way implies the occupation of these sites by specific carbon atoms, but is intended only to correlate the effect of the three molecular bonding orbitals with the molecular geometry of the complex. This interpretation is supported by these calculations which indicate that only the nearly parallel nature of the two planes may be predicted, since consideration of three sigma bonds produced a ligand plane to metal distance of 1.56~Å while the observed distance is 2.24~Å.

The possibility of $d_{\pi}^{}$ - $p_{\pi}^{}$ interaction between the oxygen atoms located at the B sites and the zirconium atom has been discussed by Hoard and Silverton²⁹ for $Zr(C_2O_4)_4^{4-}$. Due to the high net charge on the central atom and the apparently small orbital overlap these authors postulate only a small net contribution to the $Zr-O_R$ bond stability. The mean bond ratio, $Zr-O_A:Zr-O_B = 1.03$, reported for the oxalate complex is identical to that obtained in this solution. The C-O bond distances in the acetylacetonate ligands, which have less geometrical constraint than the oxalate ligands $(C-O_B/C-O_A = 1.00)$, would be expected to show the effect of delocalization of electrons about the oxygens atoms. The observed bond length ratio, $C-O_{R}:C-O_{\Lambda} = 1.03 \pm 0.01$, is in agreement with these expectations and indicates sufficient $\mathbf{d}_{\pi}^{}-\mathbf{p}_{\pi}^{}$ interaction to produce a geometric effect. The contribution of the d_{π} -p $_{\pi}$ interaction to the bond stability of the $Zr-O_{\rm p}$ bond is probably minor since the fold observed for the acetylacetonate-metal bond would be expected to decrease the effective overlap of these orbitals.

The molecular configuration of π -C₅H₅(C₅H₇O₂)₂ZrCl may be correlated reasonably well to the dodecahedral model frequently associated with the stereochemistry of eight

co-ordination. This assignment has been based upon the geometry characterized by the five unambiguously defined co-ordination sites, by the position of the zirconium atom with respect to these sites, and by the orientation of the plane of the cyclopentadienyl ring. No attempt has been made to associate specific carbon atoms of the ligand with the three co-ordination sites assigned to the ring.

The dodecahedral description of the geometry of this complex presents some interesting possibilities for stereo-isomerism and has contributed to the initiation of an investigation of these possibilities.¹¹

V. INTRODUCTION

The preparation and characterization of nonstoichiometric systems are currently topics of considerable interest.

Nonstoichiometric systems result from substitution within
the crystal lattice of either mixed cationic oxidation
numbers or different valent anions exhibiting similar crystal radii. Examples of both types of nonstoichiometric
phases may be found in the chemistry of the lanthanide elements, some of which have been studied extensively.

Perhaps the most thoroughly investigated nonstoichiometric oxide system is that of praseodymium. The phase diagram for this system, which has been reported by Hyde et al.³⁷ displays several discrete ordered phases in the composition range PrO_{1.7} to PrO_{1.8}. The nonstoichiometrically related phases appear to reflect the flexibility of the parent fluorite lattice displayed by PrO₂. This praseodymium system may be described by an anion vacancy model which compensates for substitution of Pr³⁺ ions for Pr⁴⁺ions by creation of an appropriate number of anion vacancies. Eyring and co-workers^{38,39} have indicated that the symmetry of the parent lattice varies from triclinic to rhombohedral as a result of slight shifts in the metal ion positions.

Nonstoichiometry has been reported in ternary systems possessing anions of unequal valence, for example, the lanthanide oxide fluorides. These compounds also exhibit a fluorite related structure. For example, stoichiometric samarium oxide fluoride crystallizes with rhombohedral symmetry which Zachariasen has related to the fluorite lattice. Brauer and Roether have recently reported the existence of a number of complex phases which may be described by the formulation: SmO_nF_{3-2n} where n=0.80 to 0.84. They reported that these phases, which have not been completely characterized, apparently exhibit one lattice parameter of three to seven times the nominal fluorite value. Mechanistically, the oxide fluorides may be described in terms of an interstitial anion model with a constant valent cation lattice.

The preparation of $SmF_{2.29}$ by reduction of SmF_3 with hydrogen has been reported by Asprey et al.⁴⁴, and the existence of a cubic mixed fluoride phase of variable composition was postulated. It seemed probable that a system exhibiting a considerable range of nonstoichiometry might be obtained by further reduction of SmF_3 and that this system should comply with a still third mechanism for modification of the fluorite lattice. This mechanism may be considered most easily by starting with the fluorite SmF_2 lattice. For each Sm^2 ion replaced by a Sm^3 ion an interstitial fluoride ion should be added to the lattice, and thus this Sm(II)-(III) fluoride system should resemble the variable

cationic lattice of the oxides and also display the interstitial anion behavior of the oxide fluorides.

The uranium-oxygen system has characteristics which indicate some similarities with this fluoride system. Uranium dioxide displays fluorite symmetry and a considerable range of nonstoichiometry has been reported for the uranium oxygen system. In particular, the UO2-UO3 portion of the system may be expected to comply with a similar interstitial anion model. Both the higher ionic charges of these ions, which may produce more ordering in the defect lattice, and the greater difference in their crystal radii, may make the uranium oxide system more complex than the samarium fluoride analog, however, the expected similarities should permit a meaningful comparison between these systems.

The reduction of SmF_3 with graphite, molybdenum, or tungsten was investigated by Kirshenbaum and Cahill⁴⁷, but in each case the reducing agent was found to be less effective than hydrogen. These observations indicate the need for a more active reducing agent than hydrogen; consequently, the reaction between elemental samarium and SmF_3 was investigated.

VI. EXPERIMENTAL

Preparation of Samarium Trifluoride

Samarium trifluoride, one of the reactants for preparation of the reduced fluorides, was prepared by reaction of Sm₂O₃ (99.9% theoretical samarium content, Michigan Chemical Corp.) with gaseous anhydrous HF (99.9% minimum purity, The Matheson Company, Inc.) diluted with nitrogen. The sesquioxide, contained in a platinum boat and calcined at 800-8500, was inserted into a nickel tube lined with platinum foil in the center of the heat zone (Figure 16). The system was flushed with nitrogen for one half hour before the HF flow was initiated. After the mixed HF/N_2 atmosphere was established, the nickel tube was heated: first to 2500 for two to three hours, and then to 500° for approximately ten hours. The sample was cooled to room temperature under the mixed gas atmosphere, after which the HF flow was terminated and the system flushed with nitrogen for at least one hour. The product was weighed, recycled to check for constant weight, and subsequently stored in platinum in a vacuum desiccator. The samarium trifluoride was analyzed for samarium and a powder X-ray diffraction pattern (hereafter called powder pattern) was obtained.

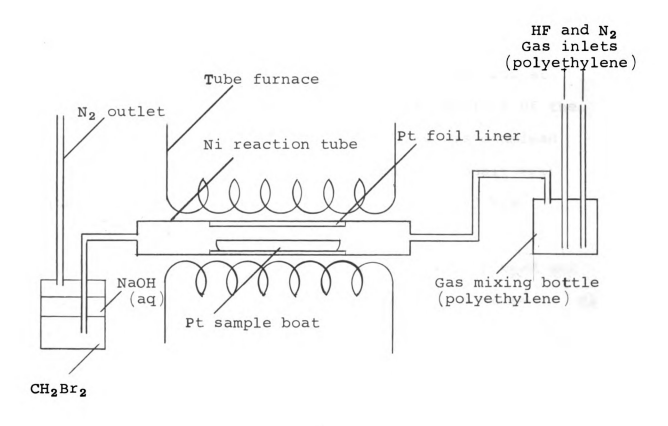


Figure 16. Schematic representation of the ${\rm SmF_3}$ preparation line.

Preparation of the Reduced Samarium Fluorides

Two closely related techniques were employed for preparation of the reduced fluorides: a) direct reaction of the metal with the trifluoride and b) subsequent reaction of the product from (a) with either elemental samarium or the trifluoride. Due to the high vapor pressure of samarium and the desirability of obtaining fused samples, the reactions were effected in tantalum bombs.

Tantalum tubes (6.2 or 9.0 mm i.d., 0.4 mm wall), from which the reaction bombs were constructed were outgassed by induction heating under vacuum (approximately 10^{-6} torr) to a minimum temperature of 2100^{0} (optical pyrometry, emissivity corrected but no transmittance correction) for at least three hours. After heating, the inner surface of the water cooled Vycor jacket of the vacuum line was examined for a metal deposit. The presence of such a deposit was considered as an indication that the tantalum had been sufficiently outgassed.

One end of the outgassed tantalum tube was crimped and sealed by arc welding in an argon atmosphere. Because of the susceptibility of tantalum to reaction with oxygen at high temperatures, considerable effort was expended to purge the welding apparatus of air. A mechanical vacuum pump (Cenco Hyvac 2, Central Scientific Co.) evacuated the system to about 0.01 torr after which it was flushed with argon three times, and then filled to a positive pressure with this gas. A zirconium button (which served as an

oxygen getter) was first arced and then the tantalum tube welded under this positive argon pressure. A very clean, shiny weld was generally obtained by this technique. However, if any sign of discoloration was detected after welding, the tube was subjected to further outgassing.

The tantalum tubes were charged with the appropriate reaction mixture in a controlled-atmosphere glove box. The argon atmosphere of this glove box was recirculated over activated alumina to remove water and over BASF Catalyst R3-11 (Badische Anilin-& Soda-Fabrik A.G.) to remove oxygen. Samarium metal (99.6% lot analysis, Michigan Chemical Corp.), which was stored under xylene when not in the glove box, was chipped from an ingot with a carbon steel cold chisel (the fragments were subsequently checked for steel particles with a permanent magnet), rinsed with trichloroethane and stored in the glove box until needed (less than one week).

The procedure employed in charging reaction vessels with sample depended on the preparative technique used. When reaction between the trifluoride and the metal was employed the trifluoride powder was first weighed into the open bomb. The powder was inserted through a small funnel whose delivery tip was at least two centimeters below the top of the tube and was subsequently packed tightly so that it was in the lower portion of the bomb. The tantalum tube was crimped tightly against the sample after it had been charged with the appropriate quantity of samarium. The charged bomb was then transferred to the arc welder via an argon

filled desiccator. A slightly different procedure was employed when one of the reactants was a reduced samarium fluoride. The reduced fluoride was first weighed into the bomb (generally the smaller diameter tube) and the stoichiometry of the mixture was adjusted with the appropriate quantity of either the trifluoride or the metal.

The charged tantalum tubes were then sealed by arc welding as described previously and the welds were examined for discoloration or obvious faults. If a weld appeared unsatisfactory (usually indicated by discoloration) the sample was discarded.

The bombs were heated under vacuum to 1600-1900° depending on the composition of the reaction mixture. In the initial stages of this investigation samples were maintained at temperature for about five minutes and quenched, however, since the powder patterns were diffuse, sample annealing was initiated.

Two annealing techniques were employed in the course of this investigation. A group of four samples was heated to 1900° until the bombs expanded, after which the temperature was lowered to 1200° over a period of four hours, and then to room temperature over a two-hour interval. These samples were then transferred to a quartz tube (lined with tantalum foil in the sample region) for further annealing. The quartz tube was evacuated (10^{-6} torr) and heated subsquently to 1200° (Pt-10% Rh thermocouple, Honeywell Potentiometer) in a Marshall platinum-40% rhodium wound tube furnace

(National Research Corp). After the temperature had been maintained at 1200° for eight hours, it was lowered to room temperature over an interval of approximately one hundred hours. Since minor golden discoloration was observed on the tantalum bombs annealed in this manner, subsequent annealing was effected in the vacuum system used for preparation of samples. After samples had been heated to 1900° as part of the initial preparation, they were cooled to 1200°, maintained there for about eight hours, and then brought to room temperature with stepwise cooling over a period of about fifty hours. The temperature control was considerably less rigorous when samples were annealed in this manner but there was no detectable discoloration.

All bombs were opened with a tubing cutter under the argon atomosphere of the glove box and the product removed by fracturing the solidified melt. The product was generally powdered in the glove box with an agate mortar and pestle and placed in dried glass vials which were sealed with paraffin wax upon removal from the box.

One sample was placed in an outgassed tantalum tube and the top was crimped tightly but not welded. This sample was heated to 1150° for five minutes, quenched, removed from the vacuum line after thorough cooling, and immediately placed in the glove box. The water cooled jacket of the vacuum line was washed with $6\underline{N}$ HCl to determine the reactivity of the condensed effusate.

Vapor Transport Experiments

A portion of one of the initial products was placed in an outgassed tungsten effusion crucible to examine its vaporization behavior. After the sample had been heated for about two hours at 1100° (black body temperature measured with an optical pyrometer, no transmittance correction), it was cooled thoroughly and examined. A deposit which was identical in appearance to the residue had condensed on the lid.

The above observations led to a decision to attempt crystal growth by a vapor phase transport technique. Consequently, a sample was placed in an outgassed tantalum tube and a bomb prepared in the usual manner. This bomb was placed in the vacuum line and the induction heating coil was positioned so that the lower end of the bomb was centered in the coil. The sample was then heated for about five hours with the furnace power adjusted to produce a temperature of approximately 1200° over the sample region of the bomb. The temperature of the upper portion of the bomb was estimated by optical pyrometry to be 900-1000°. The product, removed from the walls of the bomb by scraping the surface with a needle, was examined subsequently with a microscope by placing the material under paraffin oil and using reflected light.

Powder X-Ray Diffraction Patterns

A Guinier focusing powder X-ray diffraction camera equipped with a fine focus copper X-ray tube (Figure 17), acquired during the course of this investigation, was used to obtain powder patterns of the various products. This camera has an effective radius of 80 mm, which when combined with its focusing character results in better resolution than that obtainable from the previously available 114.7 mm Debye Scherrer cameras. Even greater resolution is possible by extremely precise adjustment of the monochromator (a quartz crystal cut at 3° to the $(10\overline{1}1)$ plane and ground to a radius of 500 mm) and the primary beam slits for elimination of the K_{Ω_2} radiation. This precise alignment (very difficult due to lack of reproducibility in the necessary adjustments of the camera) has not yet been accomplished successfully.

In order to obtain the maximum accuracy in the lattice parameters obtained from the Guinier films, an internal standard is used to calibrate the film cassette and compensate for film shrinkage. Potassium chloride (a = 6.29300 \pm 0.00009 648 , 250), which had been annealed at 600^{0} after pulverizing, was used as the internal standard in this investigation.

Both the sample and a small amount of KCl were secured to the planchet with amorphous plastic adhesive tape and, in the case of long exposures, were covered with a thin

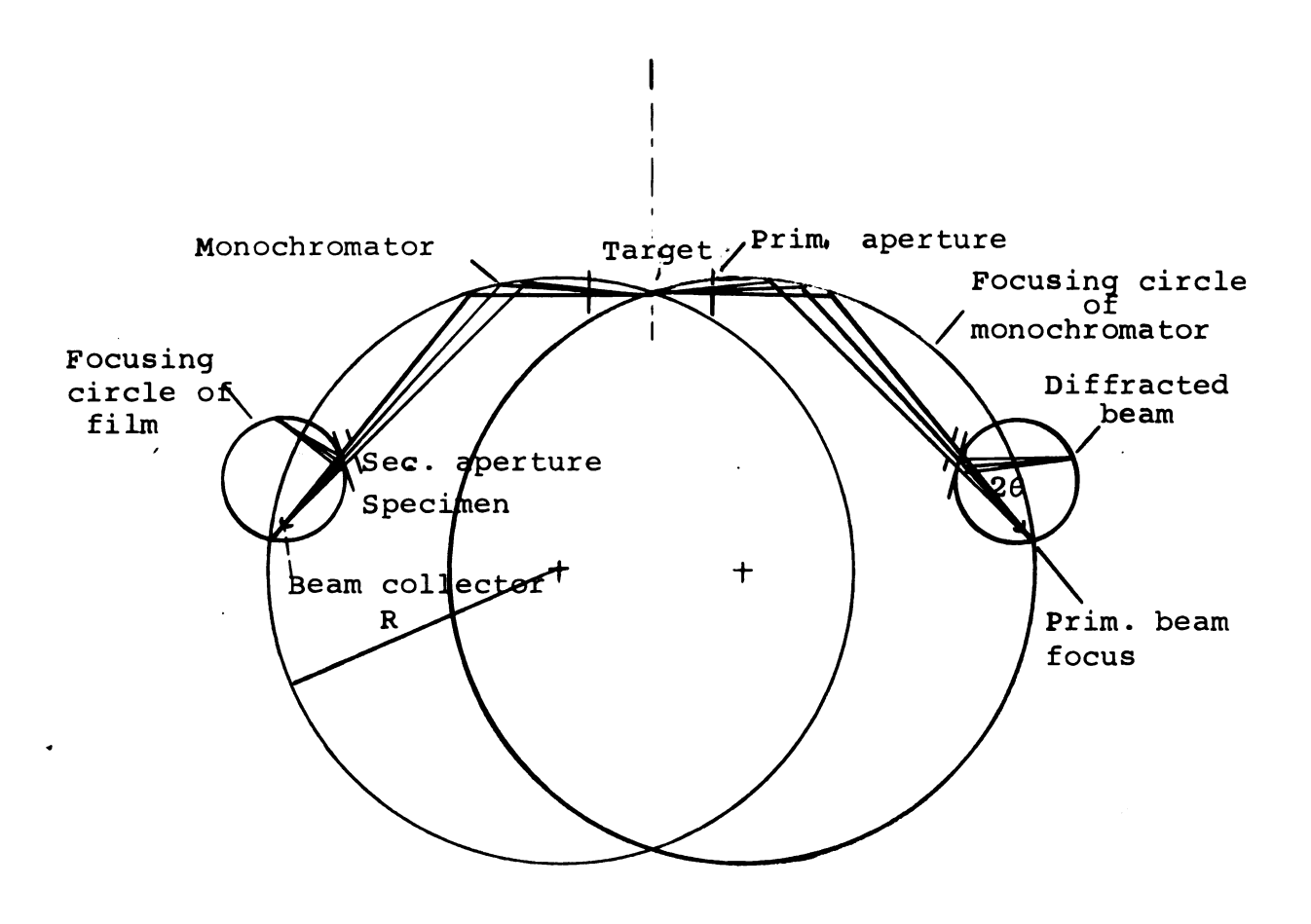


Figure 17. Schematic of the Guinier camera.

coat of paraffin oil to minimize hydrolysis, which occurred upon prolonged exposure to air. The planchet (a steel disc with 5mm hole in the center) was placed in the holder, a slowly revolving magnet, with the back side of the tape against the magnet. The film cassette, which contained a 20 x 140 mm strip of Illford Type G Industrial X-ray film encased in two sheets of paper to prevent light exposure, was placed on the pin point triangular support of the camera box. With the incident beam stop on the film cassette open, the camera box was closed for safety purposes, and the shutter on the X-ray tube was opened to expose the film to the incident beam. After this exposure (about one second) the beam stop on the cassette was closed and the camera box was evacuated with a mechanical pump (Hyvac 7). The films were exposed four to twelve hours (35 kilovolts at 20 milliamperes, Picker Nuclear X-Ray Generator). The procedure used to process the Guinier photographs differs from that normally employed. Due to the sharp lines obtained and angle of intersection of the diffracted beam with the film, two noncoincident images are recorded, one on the inner layer of the emulsion and the other on the outer layer. Consequently one layer of emulsion must be removed (usually the outer layer), and this was accomplished with a tooth brush after the film had been desensitized by the fixing solution and before it had cleared.

Determination of the lattice parameters for the samarium fluoride samples required precise reading of these powder

patterns. The recommended procedure utilizes a scale calibrated to the nearest 0.1 mm photographically printed directly on the film and read by projection on a screen. Unavailability of the scale necessary for the photographic reproduction resulted in use of a Picker X-ray film reader calibrated for direct reading to the nearest 0.01 mm. Unfortunately this apparatus is subject to parallax errors.

The film shrinkage - cassette calibration was obtained graphically from a plot of ΔS \underline{vs} . S for the KCl powder pattern, where S is the observed distance from the index (the incident beam image) to the diffraction line and ΔS is the difference between the observed and theoretical distances. The linearity of this correction (Figure 18) was very reproducible, however, its magnitude varied from film to film. $\sin^2\theta$ values corresponding to the corrected S values were obtained from an appropriate table, and refined lattice parameters were obtained from the indexed $\sin^2\theta$ values by application of a least squares linear regression program written by Lindqvist and Wengelin⁴⁹.

Analysis

Each reaction product, including SmF₃, was analyzed for samarium by steam hydrolysis to the sesquioxide. Three 0.2 g samples (two samples were used when only small quantities were available) were weighed into platinum boats and placed in a 25 mm Vycor reaction tube. Heating was initiated after a steam generator had been connected to this tube.

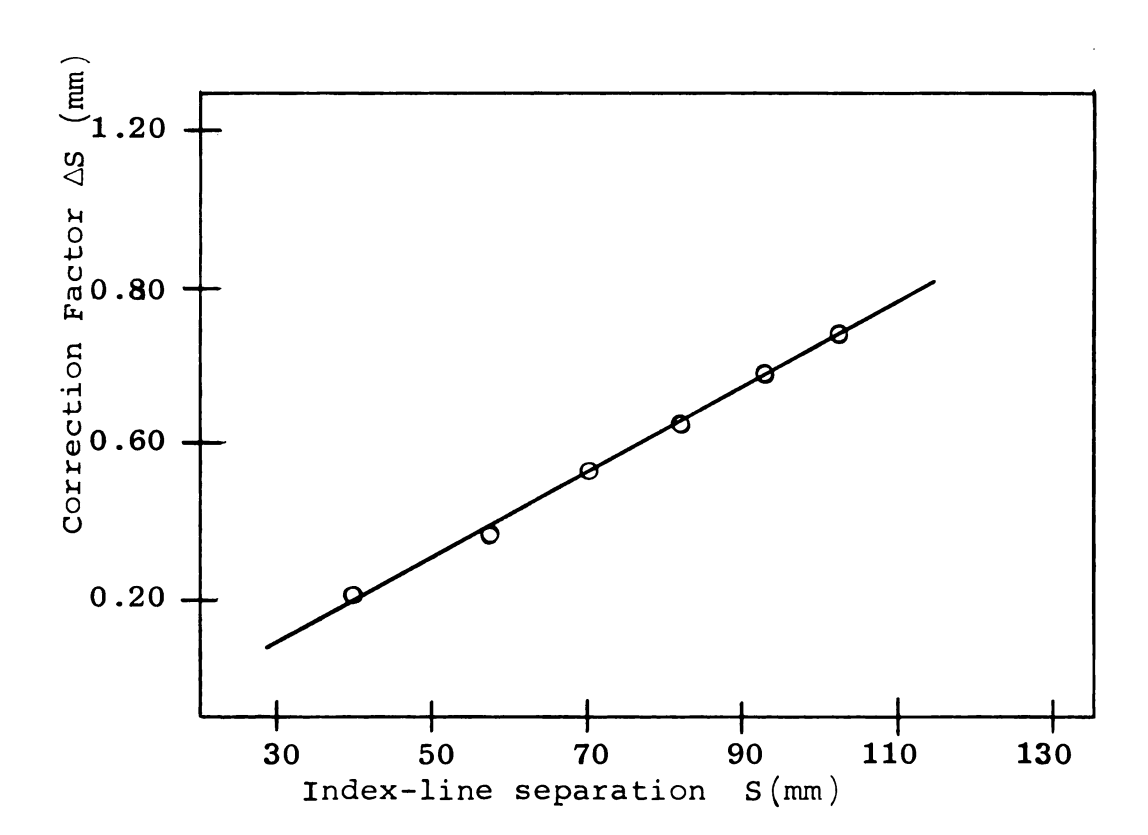


Figure 18. A typical film cassette-shrinkage correction for Guinier photographs.

The steam flow rate was such that one to one and one-half liters of water evaporated in a twelve-hour period. In about two hours the temperature of the reaction tube attained 1000° where it was maintained for at least six hours. The samples were cooled in air and subsequently placed in a 900° muffle furnace to drive off any absorbed carbon dioxide, recooled in a vacuum desiccator, and weighed. Several samples were checked for constant weight by recycling them through the preheated hydrolysis line for two hours.

In an effort to determine the magnitude of oxygen contamination in the reduced samarium fluorides several samples were sent to National Spectroscopic Laboratories (Cleveland, Ohio). Their oxygen analysis was effected by the platinum-carbon fusion technique. The presence of fluorine generally produces erroneous results due to the formation of fluorocarbons, however, the procedure employed at their laboratory was modified in an attempt to obtain satisfactory results.

Density

The density of the reduced samarium fluorides was determined pycnometrically with $\mathrm{CH_2Br_2}$ as the solvent. The volume of the pycnometer, which was equipped with a thermometer for monitoring solvent temperature, was calibrated with boiled distilled water and the density of the methylene bromide was determined subsequently as a function of temperature. Only a small volume of product was available, thus all weighings were made to the nearest $0.01~\mathrm{mg}$ on an automatic Mettler (Mettler Instrument Corp.) semi-micro balance.

A well-powdered sample was poured into the pycnometer through a funnel to avoid contact of the powder with the ground glass joint. The sample and pycnometer were weighed quickly and solvent was introduced in an effort to minimize exposure of the sample to air. The pycnometer, containing the sample and about half filled with solvent, was placed in a vacuum desiccator and subjected to reduced pressure. Approximately one cubic centimeter of solvent was pumped off in an attempt to remove adsorbed gases from the powder surface.

After the pycnometer had equilibrated to room temperature, it was filled with solvent. The temperature of the pycnometer generally increased by a couple of degrees when it was wiped to remove excess solvent, and thus several measurements were effected as a function of temperature while it cooled. Weighings were made on a dynamic system, since solvent was evaporating continually. Formation of a meniscus on the side arm was taken as the reference point for all weighings and the temperature was read immediately after the weight was obtained. At least ten weight-temperature measurements were obtained for each density determination.

VII. RESULTS

Samarium Trifluoride

Several samples of samarium trifluoride were prepared during this investigation and in each preparation the product was a fine white powder. The weight changes during the reaction (99.9 \pm 0.1% theoretical) as well as the samarium analyses (99.9 \pm 0.2% theoretical) were indicative of complete conversion to the trifluoride. The Guinier photographs obtained from these samples displayed lines corresponding to both the hexagonal and orthorhombic crystal forms. 50 , 51

Physical Appearance of the Reduced Samarium Fluorides

The physical appearance of the reduced samarium fluorides varied as the composition was adjusted from SmF_2 to $SmF_{2.5}$. The color of the opaque fragments obtained by fracturing the fused product was purple when the composition was near SmF_2 , but became progressively more red as the fluoride content increased and was a dull burgundy red at the composition $SmF_{2.5}$. The samples displayed a minor color change upon powdering, which required a considerably greater effort for material whose composition was near SmF_2 than for more fluoride rich samples. The purple fragments gave a

deep blue to blue-green powder while the burgundy colored samples simply appeared lighter when powdered. When viewed with transmitted light under a microscope, the powder remained opaque and subsequent examination of both fragments and powder with reflected light revealed an apparently regular change in color as a function of composition.

Microscopic examination of the fragments confirmed the presence of sharp faces, but recurrent morphology was not detected.

A number of powdered samples were exposed to $6\underline{N}$ HCl solutions and a definite increase in the rate of gas evolution was noted as the fluorine to samarium atomic ratio was decreased to two. The rate of evolution was moderate for SmF_2 , but was considerably more vigorous when the relative samarium content was increased. Similar gas evolution was noted when $6\underline{N}$ HCl was added to the coating deposited on the Vycor jacket of the vacuum line during heating of the sample in the open tantalum tube.

Vapor Phase Crystal Growth

The appearance of the material on the walls of the tantalum bombs used for vapor phase transport indicated the probable existence of single crystals. When light was directed into the top portion of the tantalum tubes bright reflections were noted as the tubes were rotated.

The material, when observed under a microscope, was found to consist mainly of fine powder; however, a couple

of small crystals were detected. One crystal in particular displayed very sharp faces and was selected for examination with single crystal techniques. A considerable number of oscillation photographs taken of this crystal failed to allow selection of any rotation axis with the expected cubic lattice parameters. A number of equi-inclination Weissenberg photographs, taken with rotation about an axis believed to be a face diagonal of the fluorite cell, produced a set of indices which could not be transformed to the desired cubic set nor correlated with any of the crystallographic space groups. As a result the crystal was thought to be a twin and further identification was not attempted.

Analytical

The composition of the samples is displayed in terms of per cent samarium (average deviation) and stoichiometry in Table X. The fluoride content of the samples was determined by difference and consequently the precision indicated in the stoichiometry reflects only that of the metal analysis. The analytical results were consistent with the composition of the starting mixtures, and thus are believed to be reliable.

Each of two different sets of samples sent to National Spectroscopic Laboratories contained a portion of " Sm_2OF_4 " taken from the same preparative sample. A sample of CaF_2 (A.C.S. Reagent Grade) was also sent with the second set of samples. The analytical results are tabulated in Table XI,

Table X. Samarium analysis and stoichiometry

Samarium Analysis	Stoichiometry	Samarium Analysis	Stoichiometry
81.22(25)*	SmF _{1.83} (3)	77.74(03)	SmF _{2.26(1)}
79.83(06)	$SmF_{2.00}(1)$	77.50(08)	SmF _{2.29(1)}
79.78 (17)	$SmF_{2.01}(2)$	77.31(13)	SmF _{2.32(2)}
79.78(05)	SmF _{2.01(1)}	77.09(06)	SmF _{2.35(1)}
79.58(05)	SmF _{2.03} (1)	76.99(10)	SmF _{2.36(1)}
79.26(05)	SmF ₂ .07(1)	76.77(04)	SmF _{2.39(1)}
79.01(07)	SmF2.10(1)	76.68(09)	SmF _{2.41(1)}
78.71(04)	SmF _{2.14} (1)	76.67(09)	SmF _{2.41(2)}
78.52 (07)	SmF _{2.17(1)}	76.45(09)	SmF _{2.44(1)}
78.31(06)	SmF _{2.19(1)}	76.25(05)	SmF _{2.46(1)}
77.89(13)	SmF _{2.24(2)}	75.73(03)	SmF _{2.54(1)}

The numbers enclosed in parentheses are the average deviations.

Table XI. Oxygen analyses obtained from National Spectroscopic Laboratories (Cleveland, Ohio)

	% 0 (wt) Set I	% O (wt) Set II
"Sm ₂ OF ₄ " (Pt)*	4.26	4.69
"Sm ₂ OF ₄ " (Ni)	-	3.82
CaF ₂	-	3.09
$SmF_{\mathbf{x}}$	0.24(04)**	0.38(00)**

^{*} A portion of the sample prepared in the platinum boat was sent with both sets of samples.

^{**}The values included in the parentheses are average deviations.

and it is apparent from the inconsistency in the $"Sm_2OF_4"$ analyses and the high results obtained for CaF_2 that the procedure used was inadequate. The oxygen content has not been adequately analyzed; however, the precautions taken to avoid oxygen contamination were extensive and therefore the samples are believed to contain considerably less oxygen than these results indicate.

Density

The volume of the pycnometer, as determined from the tabulated 52 absolute density of water, was found to be $9.7990 \pm 0.0001 \, \mathrm{cm^3}$ at 24° . The measured density of the A.C.S. Reagent Grade methylene bromide used as the solvent is displayed graphically as a function of temperature in Figure 19.

The small volume of fluoride samples available for these measurements limited the precision of the density determination. For example, a deviation in sample volume of 0.0004 cm³, a typical value, produced as much as 0.02 g cm⁻³ deviation in the measured density. The measured densities and their standard deviations are contained in Table XII.

Unit Cell Symmetry and Lattice Parameters

Guinier powder patterns taken of samples throughout the composition range displayed considerable similarity to the pattern obtained for the face centered cubic SmF_2 . The $\sin^2\theta$ values obtained from these photographs are listed in

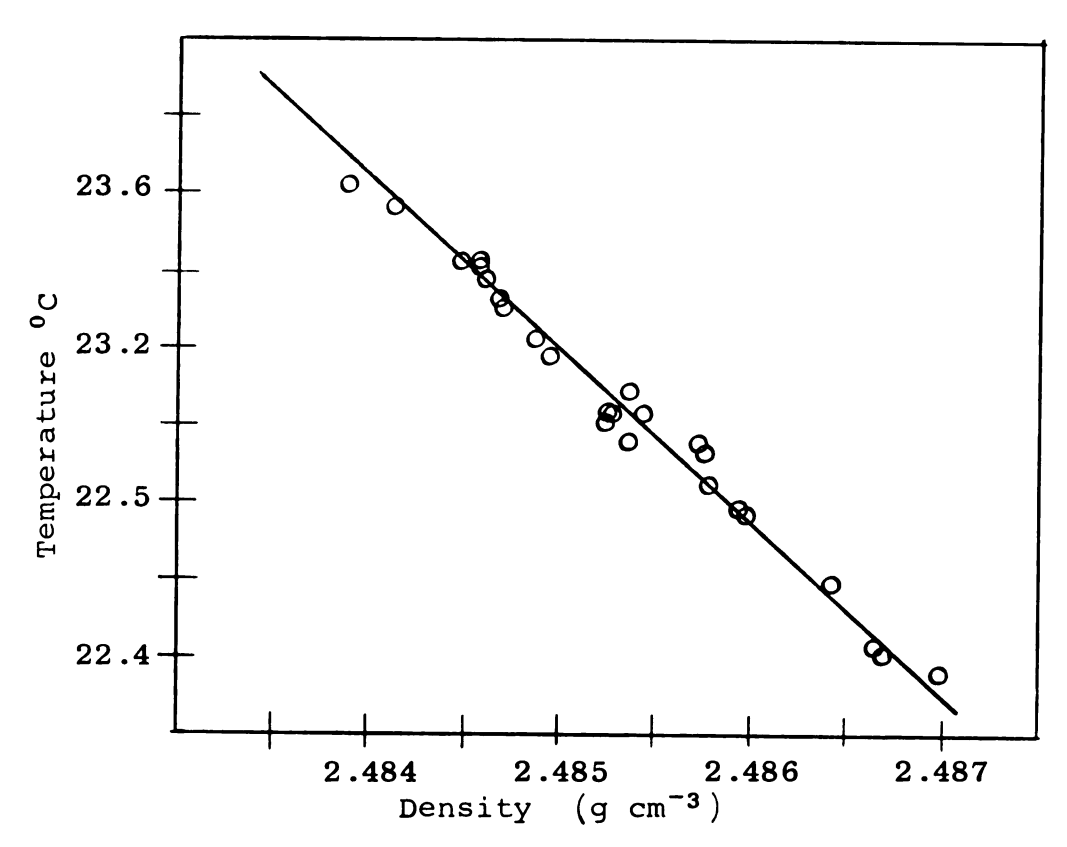


Figure 19. Density of CH_2Br_2 as a function of temperature.

Table XII. Density of reduced samarium fluorides

Composition	Density (g cm ⁻³)
SmF _{2.01}	6.16(5)*
SmF _{2.10}	6.22(2)
SmF _{2.24}	6.37(2)
SmF _{2.32}	6.55(5)
SmF _{2.36}	6.57(2)
SmF _{2.39}	6.57(2)
SmF _{2.41}	6.58(4)
SmF _{2.44}	6.73(2)

^{*}Values given in parentheses are the standard deviations based on a minimum of ten measurements.

Appendix III. Powder patterns obtained from the quenched and annealed samples displayed few significant differences. The most pronounced change, as was expected, was the sharpness of the lines. Lines obtained from annealed products were sharper than those obtained from quenched samples; these sharper powder patterns were used in the analysis of the unit cell symmetry and for lattice parameter determinations.

The powder patterns obtained for samples with an atomic ratio F:Sm of less than 2.00 were generally rather diffuse; however, they were identical in appearance to those of SmF_2 and the lattice parameters obtained from the sharpest of these photographs are the same as those of the stoichiometric compound. A cubic phase, as determined from the Guinier photographs, was found for the composition range $SmF_{2.00}$ to $SmF_{2.14}$. The cubic lattice parameters for this phase were observed to decrease as a function of composition and are listed in Table XIII.

The Guinier photograph obtained from a sample with composition $SmF_{2.17}$ contained the first indication of deviation from the cubic symmetry of the parent lattice. This powder pattern (the first one displayed schematically in Figure 20) contained doublets for each of the lines normally produced by the cubic samples. As is indicated in the figure similar powder patterns were obtained for samples throughout the region of stoichiometry: $SmF_{2.17}$ to $SmF_{2.32}$; but a trend in the relative intensities of the lines was noted (Figure 20). The powder patterns obtained from two samples, $SmF_{2.35}$ and

Table XIII. Lattice parameters as a function of composition for a reduced samarium fluoride phase

Lattice Parameter a cubic (A, 24°) 5.876(1)* 5.868(1)
` ,
5.868(1)
5.867(1)
5.870(2)
5.865(1)
5.855(2)
5.853(2)
5.845(2)

^{*}Values given in parentheses are the standard deviations determined from application of a least squares linear regression program. 48

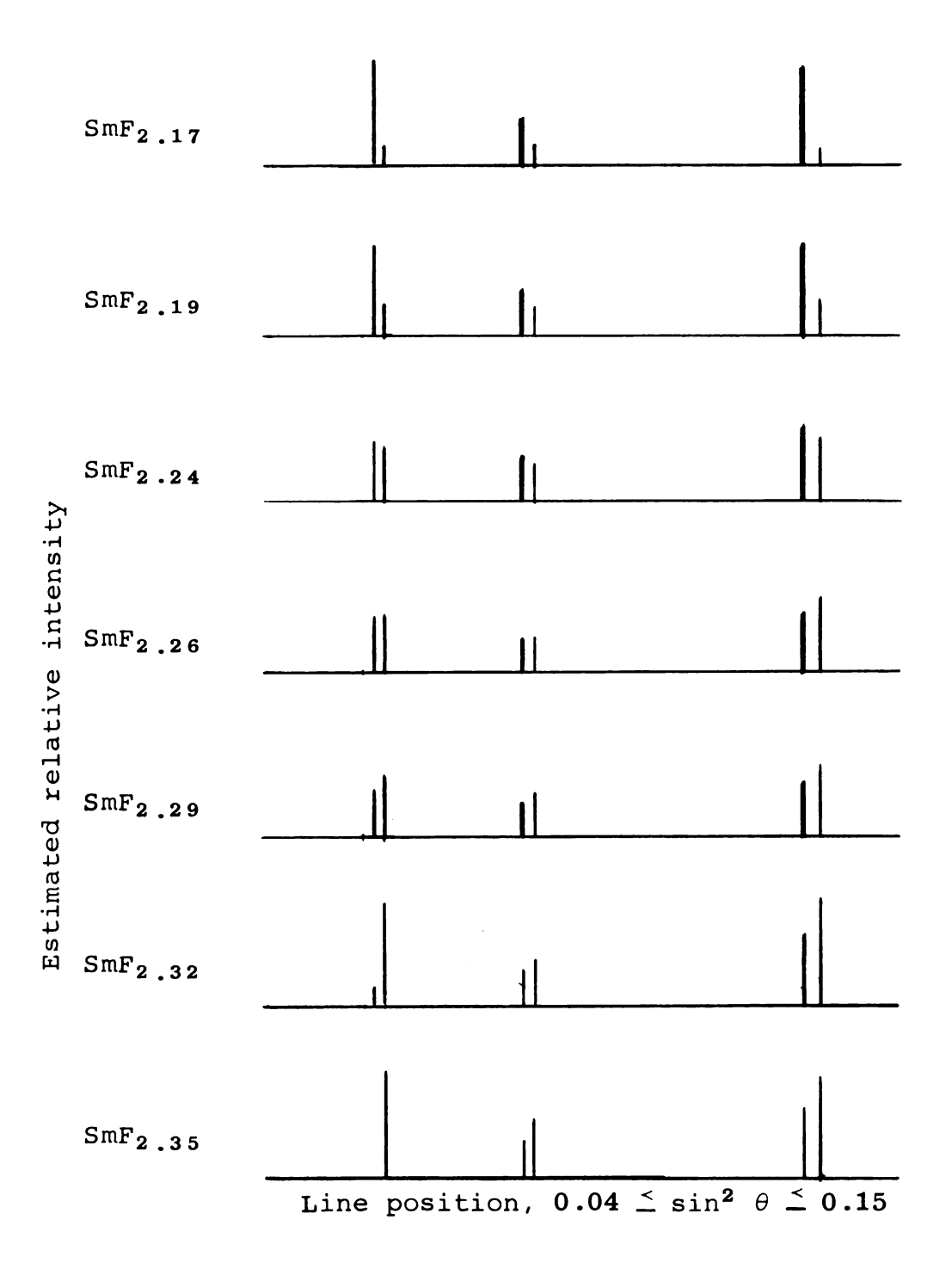


Figure 20. Estimated relative line intensity from powder patterns obtained from samples in the composition range $SmF_{2.17}-SmF_{2.35}$.

SmF_{2.36}, contained lines with the same $\sin^2\theta$ values as several of those described above and were indexed on the basis of a tetragonal unit cell with lattice parameters of a = 4.106 ± 0.002 and c = 5.825 ± 0.003 Å. A number of very weak lines (indicative of superstructure) were observed in the powder patterns obtained throughout the latter half of the stoichiometry range, but were not assignable to the tetragonal unit cell. Further examination of the strong lines in the Guinier powder patterns obtained from samples in the above composition range allowed identification of a face centered cubic unit cell with a = 5.841 ± 0.002 Å. The relative intensities of the lines associated with only the cubic phase decreased as the fluoride content increased.

When the atomic ratio F:Sm was increased from 2.36 an additional change was observed in the Guinier photographs. The new powder pattern was indexable on rhombohedral symmetry. Only one sample, $SmF_{2.39}$, produced lines that were assignable uniquely to both the tetragonal and rhombohedral phases. Samples with compositions between $SmF_{2.41}$ and $SmF_{2.46}$ produced X-ray powder patterns which were also indexable on the rhombohedral unit cell, but which produced a systematic variation in their lattice parameters (Table XIV), indicative of a continuous decrease in unit cell volume.

The powder pattern obtained from a sample of ${\rm SmF_{2.54}}$ displayed the lines of the rhombohedral phase and of samarium trifluoride. The lattice parameters obtained for the

rhombohedral phase in the two phase mixture were the same as those found for $SmF_{2.46}$.

Table XIV. Rhombohedral unit cell parameters as a function of composition

Composition	a (Å)	α (deg)
SmF _{2.41}	7.124(2)*	33.40(2)*
SmF _{2.44}	7.122(2)	33.32(2)
SmF _{2.46}	7.096(2)	33.23(2)

^{*}Values enclosed in parentheses are the standard deviations in the appropriate parameters.

VIII. DISCUSSION

The reaction between samarium and samarium trifluoride has produced a reduced Sm(II)-Sm(III) fluoride system which displays a considerable range of nonstoichiometry. The Guinier powder patterns obtained from samples throughout the nonstoichiometric range closely resemble the face centered cubic pattern obtained from SmF_2 and thus indicate that the structural behavior of this system results from modification of the parent lattice.

Fluorite Lattice

Cubic compounds possessing AB_2 stoichiometry generally display either the rutile or fluorite structure and Pauling⁵³ has determined the minimum univalent radius ratio (0.732) for which the fluorite structure has the greater stability. The univalent radius of samarium may be approximated from the trivalent radius reported by Templeton and Dauben⁵⁴ and this value, 1.27 Å, when combined with that of the fluoride ion, 1.36 Å⁵³, produced a radius ratio equal to 0.93. Thus the fluorite lattice would appear the likely model for the parent lattice in this nonstoichiometric system.

Pauling has also compared the sum of the crystal radii and the observed interionic distances for several crystals with the fluorite structure and has demonstrated their general agreement. The crystal radius of Sm^{2+} , 1.18 R,

calculated from the observed lattice parameters and the crystal radius of the fluoride ion⁵³ may be compared with that of Eu²⁺, 1.17 Å, obtained from the lattice parameters of NaCl-type EuO⁵⁵. Lee, Muir, and Catalano⁵⁶ have reported lattice parameter $a = 5.836 \pm 0.005 \text{ Å}$ for EuF₂; however, further work by Catalano and Bedford⁵⁷ has shown the actual composition to be EuF_{2.06}. If the lattice parameter-composition dependence observed for the samarium system applies to its europium analog, the lattice parameter for the stoichiometric europium difluoride would be a = 5.842 Å, a value which compares very favorably with that calculated from the above crystal radii (a = 5.843 Å). Pauling lists the crystal radius for Eu²⁺ as 1.12 Å, a value somewhat smaller than that obtained from these calculations and possibly indicative of incomplete reduction in the compounds from which it was determined.

Interstitial Anion Model

Two models based on the fluorite lattice may be proposed for a description of this nonstoichiometric system:

a) an interstitial anion model described previously, and

b) a cation vacancy model with a constant anion lattice.

The theoretical densities calculated for each of these

models from the observed unit cell volume and the observed

density are displayed graphically as a function of composition (Figure 21). It is apparent from an examination of

this figure that the cation vacancy model is not applicable to

this system and that the interstitial anion model is in agreement with the observed density behavior.

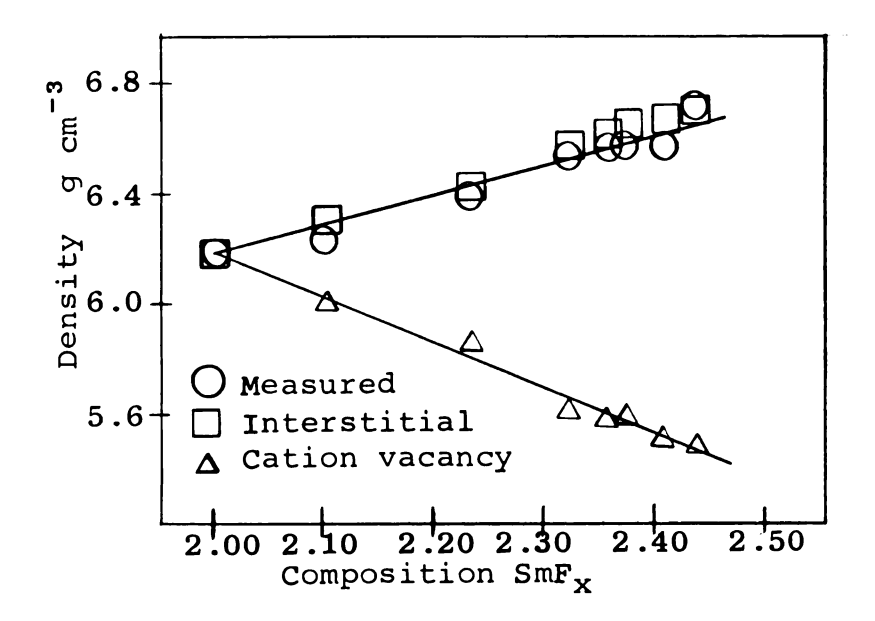


Figure 21. Density as a function of composition.

The unit cell volume decreases as the fluoride content increases. The volume-composition behavior of the interstitial anion model is governed by two opposing events:

a) substitution of a smaller and more highly charged cation with subsequent decrease of the unit cell volume and b) addition of a fluoride ion into an interstitial site with a resultant expansion of the lattice. The observed decrease

in the unit cell volume is indicative of the dominance of the substitution step in the mechanism.

An indication of the effect of addition of the interstitial fluoride ions may be obtained from an application of Vegard's law to a fluorite lattice solid solution between cations with the crystal radii of the Sm²⁺ and Sm³⁺ ions. The observed lattice parameters and those calculated from this law are displayed graphically as a function of composition in Figure 22. As is expected, the observed lattice parameters are progressively larger than those predicted.

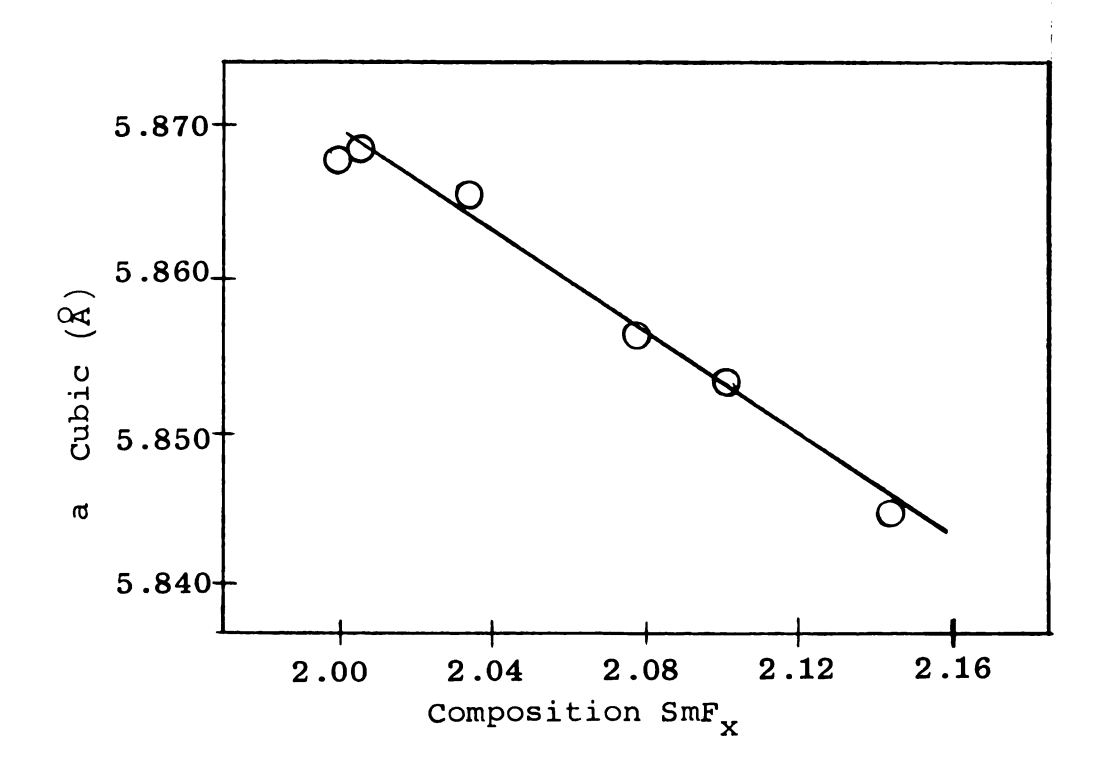


Figure 22. The effect of composition on the lattice parameters of the cubic samarium fluoride phase.

The cationic co-ordination for the fluorite lattice is displayed in Figure 23. The interstitial sites, whose effective radius equals the cationic crystal radius, are represented by open cubes. A possible description of cationic substitution and anionic addition for the present system is indicated by the arrows in this figure. The smaller size of the Sm³⁺ ion allows its displacement from the ideal cationic position of the fluorite lattice. Hard sphere contact between the trivalent samarium ions and the fluorite-type anions would result in an increase in the effective radius of the adjacent interstitial site (1.33 A)and would require less distortion of the adjacent co-ordinate polyhedra when a fluoride ion was added to the lattice at this site. The proposed geometry for the co-ordination of the trivalent cation is shown in Figure 24 along with the co-ordination sphere for SmF₃ as determined by Zalkin and Templeton. 50 The similarity between these co-ordination geometries and the culmination of the nonstoichiometric phase in a two phase region with SmF_3 serve as good supporting evidence for the proposed model.

Application of this model to the Sm(II)-Sm(III) fluoride system is based on the assumption that initial deviations from the SmF_2 stoichiometry occur by random location of the interstitial defect pairs. The regular decrease in the cubic lattice parameters appears to indicate that this mechanism can operate until the composition approaches $SmF_{2.16}$, the phase boundary determined from the cubic lattice

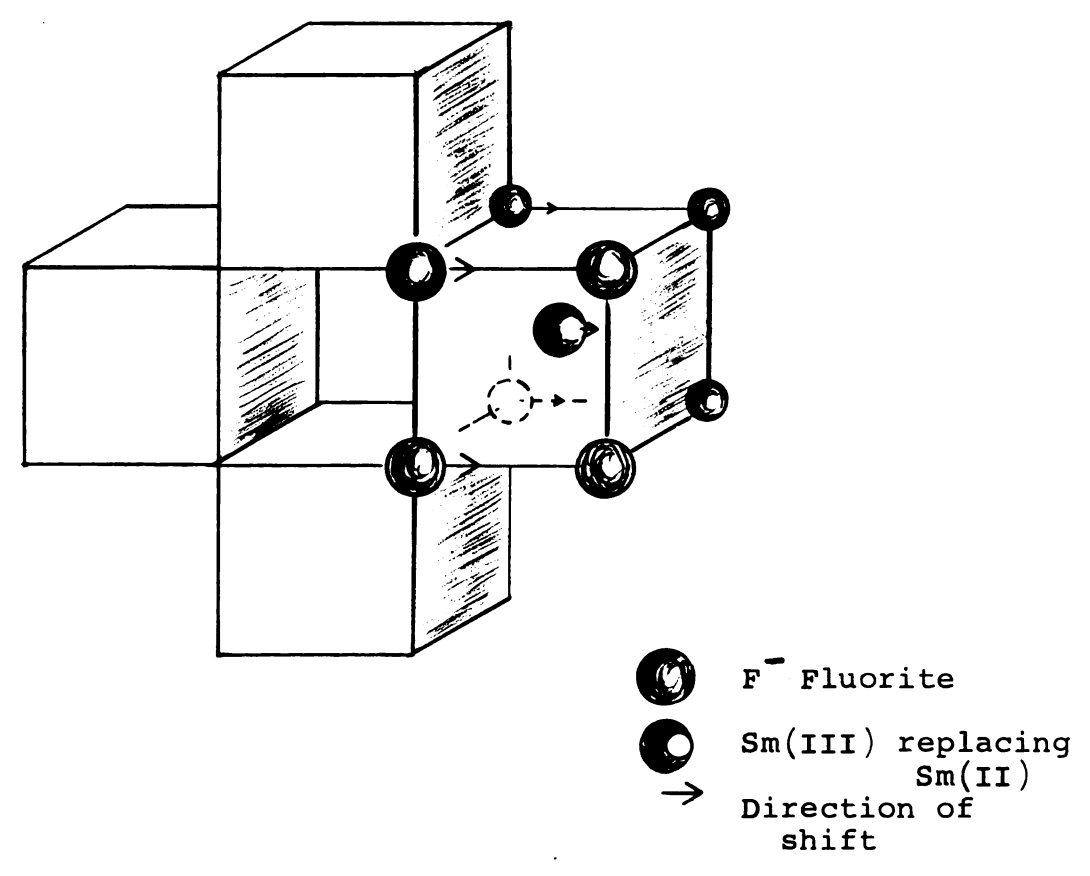
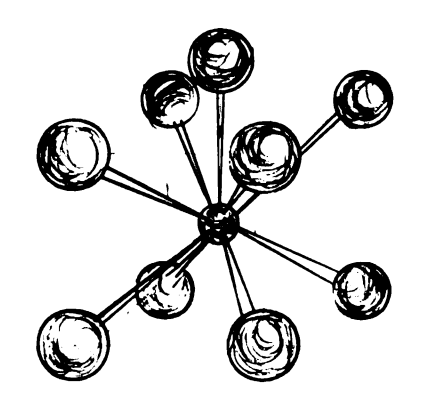
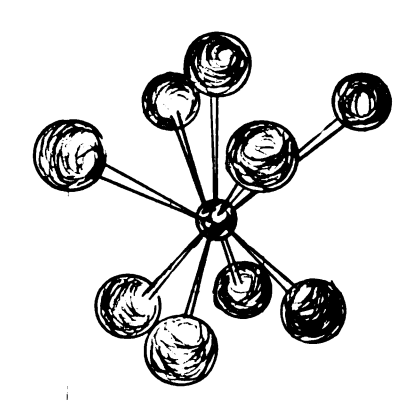


Figure 23. Samarium co-ordination in the fluorite lattice (four SmF_2 units)



a) Interstitial anion model



b) Samarium trifluoride

Figure 24. Sm(III) co-ordination.

parameters measured in the two phase region. The appearance of a nominally tetragonal phase with a narrow composition range indicates the operation of some order in the lattice, and the two phase region between the cubic and tetragonal systems may represent the region in which the random substitution mechanism gives way to an ordered substitution pro-The variation in the relative intensities of the powder pattern lines of the cubic and tetragonal phases in this two-phase region indicates the probable absence of any intermediate phases. Samarium analyses on samples whose Guinier photographs indicated only the pseudo tetragonal powder pattern (apparent superstructure lines) place its composition at $SmF_{2.35\pm0.02}$. The description of this phase as tetragonal probably reflects the pseudosymmetry of the samarium ions, since the major contribution to the X-ray scattering factors in this system is from the samarium electrons (59 and 60 vs. 10 for the fluoride ions). Consequently, the strong lines in the powder patterns should reflect the symmetry of these ions. The observed superstructure may correspond to the symmetry of the fluoride ions and therefore more closely reflect the geometry of the unit cell. Unfortunately, attempts to index these superstructure lines have not met with success.

A third phase, which also appears to be nonstoichiometric with variable lattice parameters, has been observed for samples with an atomic F:Sm ratio greater than 2.41 ± 0.01 . The powder patterns obtained from samples of this

phase have been indexed as a rhombohedral modification of the fluorite lattice. One sample, composition $SmF_{2.39}$, produced a powder pattern that contained lines attributable to both the rhombohedral and tetragonal phases and thus established a narrow two phase region between these two phases. Guinier photographs and samarium analyses indicate that the fluoride rich phase boundary is near $SmF_{2.46}$, and, as with the nonstoichiometric cubic phase, there is a regular decrease in the unit cell volume in the $SmF_{2.41}$ - $SmF_{2.46}$ region (Figure 24). Samarium trifluoride is present on the fluoride rich side of this rhombohedral phase and therefore it must be the last phase in the nonstoichiometric samarium fluoride system.

The rhombohedral geometry of the lattice at the trifluoride phase boundary may indicate the composition to be $SmF_{2.50}$ rather than the analytically determined $SmF_{2.46}$. Since no superstructure lines have been observed in the Guinier photographs obtained from these samples, the structure seems to be that of a simple rhombohedral cell. The rhombohedral unit cell (Figure 25) contains only two samarium ions, one of which is located at the body center and the other is shared between adjacent unit cells. The decrease in the rhombohedral angle, α , is consistent with the location of the trivalent ion in the body centered position; however, the interstitial sites, which would be considerably distorted, are not favorably oriented for this symmetry, and thus the probable location of the fluoride ion can not be predicted.

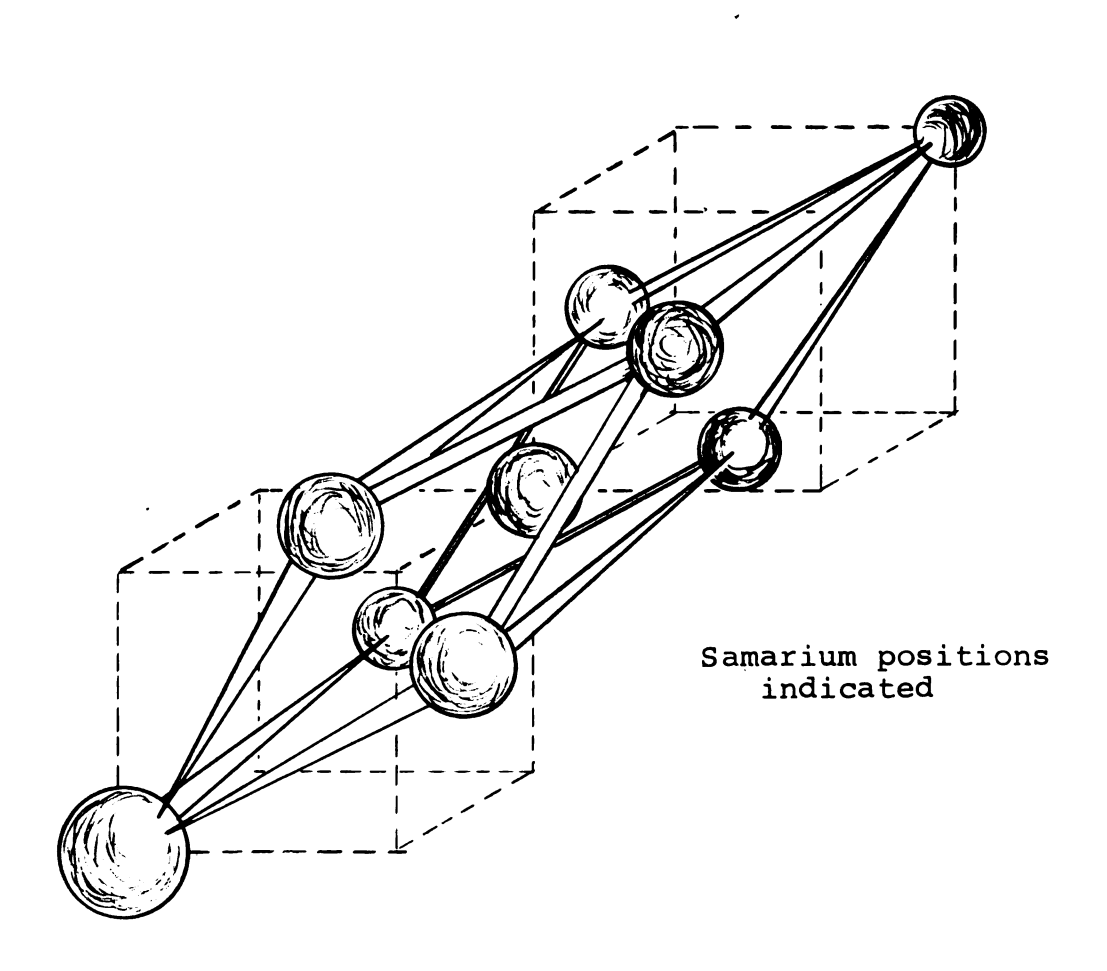


Figure 25. Fluorite related rhombohedral unit cell.

A Homologous Series

If the observed phase boundaries are considered as distinct phases, a homologous series may be constructed for this system. The general equation $Sm_{12}F_{24+n}$, where n has an integal value from 0 to 6 inclusively, will generate atomic ratios, F:Sm, in agreement, within experimental error, with the observed phase boundaries (Table XV). Two of the phases predicted have not been detected in this investigation: $Sm_{12}F_{25}$, which falls in the center of the nonstoiciometric cubic region and $Sm_{12}F_{27}$, which falls in the cubic tetragonal two phase region.

Table XV. Comparison of the stoichiometries generated by $Sm_{12}F_{24+n}$ and those observed for phase boundaries

Sm ₁₂ F _{24+n}	Observed
SmF _{2.00}	SmF _{2.00}
SmF _{2.08}	
$SmF_{2.17}$	SmF _{2.16}
SmF _{2.25}	
SmF _{2.33}	SmF _{2.35}
SmF _{2.42}	SmF _{2.41}
SmF _{2.50}	SmF _{2.46}
	SmF ₂ .00 SmF ₂ .08 SmF ₂ .17 SmF ₂ .25 SmF ₂ .33 SmF ₂ .42

If indeed the system is describable in terms of the proposed homologous series, the basic structural unit might contain twelve samarium positions which undergo substitution in an ordered manner.

Comparison with the Uranium Oxide System

Considerable similarity exists between the samarium fluoride and uranium oxide systems. A lattice parameter and density study by Lynds et al. 58 has produced results similar to those reported here. The lattice parameter for stoichiometric UO₂ (a = $5.470 \pm 0.001 \text{ Å}$), when treated with the crystal radius of the oxide ion 53 produced a crystal radius for U⁴⁺ of 0.97 Å, a value identical to that reported by Pauling. 53

The cubic lattice parameters have been found to decrease as the oxide content of the lattice increases. Lynds et al. $^{5.8}$ present two equations to describe this lattice parameter variations: one for the composition range $UO_2-UO_2._{125}$; and another for the range $UO_2._{17}-UO_2._{25}$. The first equation characterizes this behavior in terms of a nonstoichiometric UO_2 phase while the second describes a nonstoichiometric U_4O_9 phase $(UO_2._{25})$. The region described by the first equation has a clear counterpart in the samarium fluoride system (Figure 22, page 83), however, the analogy in the second range is not well defined. The region between $SmF_2._{17}$ and $SmF_2._{25}$ has been described as a two phase region containing the cubic phase, $SmF_2._{16}$, and the tetragonal phase, $SmF_2._{35}$. No significant indication of a phase with the composition $SmF_2._{25}$ has been observed in this work.

A single crystal study by Belbeoch et al. 59 has demonstrated that the unit cell of $\rm U_4O_9$ consists of sixty-four

nominally fluorite unit cells arranged in a $4 \times 4 \times 4$ array. Superstructure observed in the two-phase region and assigned to the tetragonal unit cell may in part correspond to this type of cell, however, it was not defined well enough for sufficiently accurate measurement to allow assignment. The concurrence of the phase boundary at $SmF_{2.16}$ and $UO_{2.17}$ provides some support for the existence of a phase at $SmF_{2.25}$, provided that the analogous nature of the two systems may be substantiated further.

Additional comparison between these systems may be effected by considering the homologous series, U_nO_{2n+2} , which has been proposed by Makarov. 60 This series indicates a second phase, U7016, which should have a samarium analog, ${\rm SmF}_{2,28}$, which also occurs in the cubic-tetragonal twophase region. The existence of this phase in the uranium system has not been well established, and no evidence of its analog in the samarium fluoride system has been found. The next member in the series, U₆O₁₄, has an analog in the samarium system, SmF_{2,35}, and the two phases are structurally similar. The lattice parameters of the uranium phase generally have been reported in terms of a face centered tetragonal cell. However, Hoekstra et al.61 have indicated they correspond to a body centered tetragonal cell with a = 3.78 and c = 5.55 Å. As in the samarium phase, the a parameter is less than one half the face diagonal of a cube with edge c. A modification of the tetragonal cell with a = 3.84 and c = 5.40 Å has been

observed in the uranium oxides, but no evidence for it has been found in the samarium analog.

The next phase in the homologous series U_5O_{12} ($UO_{2.40}$) has been reported to be tetragonal with a = 5.364 and c = 5.531 Å. The nearest approximation of this phase observed in this work is $SmF_{2.41}$, which has been indexed on a rhombohedral lattice. The latter indexing is consistent with the Guinier powder pattern and corresponds to a simple modification of the parent lattice.

The samarium analog of U_4O_{10} , the next phase in the homologous series, is the end of the nonstoichiometric rhombohedral phase. The uranium compound has been examined by single crystal techniques and has been found to be orthorhombic. It seems apparent that while the same stoichiometries are involved, the lattice modifications are different for the two systems. The uranium system displays at least one more phase, with several crystal modifications, before the lattice collapses to that of UO_3 , and thus appears to be more complicated at the anion rich end of the nonstiochiometric region. This complexity may be a result of the different charges and size of the ions.

It is apparent from the above discussion that the non-stiochiometry displayed by these two systems is the result of similar modifications of the fluorite lattice. While the present investigation of the Sm(II)-Sm(III) fluorides has not established the nature of these changes, it may have provided an alternative path to their illucidation.

IX. SUGGESTIONS FOR FUTURE RESEARCH

The Sm(II)-Sm(III) fluoride system displays a wide range of nonstoichiometry and undergoes a number of lattice modifications. Its similarity with the uranium oxygen system has been discussed. In view of these similarities, an understanding of both of these systems would benefit from a systematic examination of the samarium fluorides by single crystal X-ray diffraction techniques, with a detailed structural analysis as the primary goal. The samarium system is better suited to application of the heavy atom technique than the uranium analog since uranium (88 and 86 electrons) would dominate the structure factor more than samarium would.

Vapor phase transport experiments conducted during this investigation indicate that single crystals may be obtained by this method. Attempts to apply this technique to crystal growth may be facilitated by a consideration of the following procedure.

Place about one gram of sample in an outgassed tantalum tube and flatten the container to reduce its volume. This flattening will reduce the argon pressure in the bomb and increase the mean free path length. Once the tube has been sealed, it should be heated <u>in vacuo</u> to about 1800°;

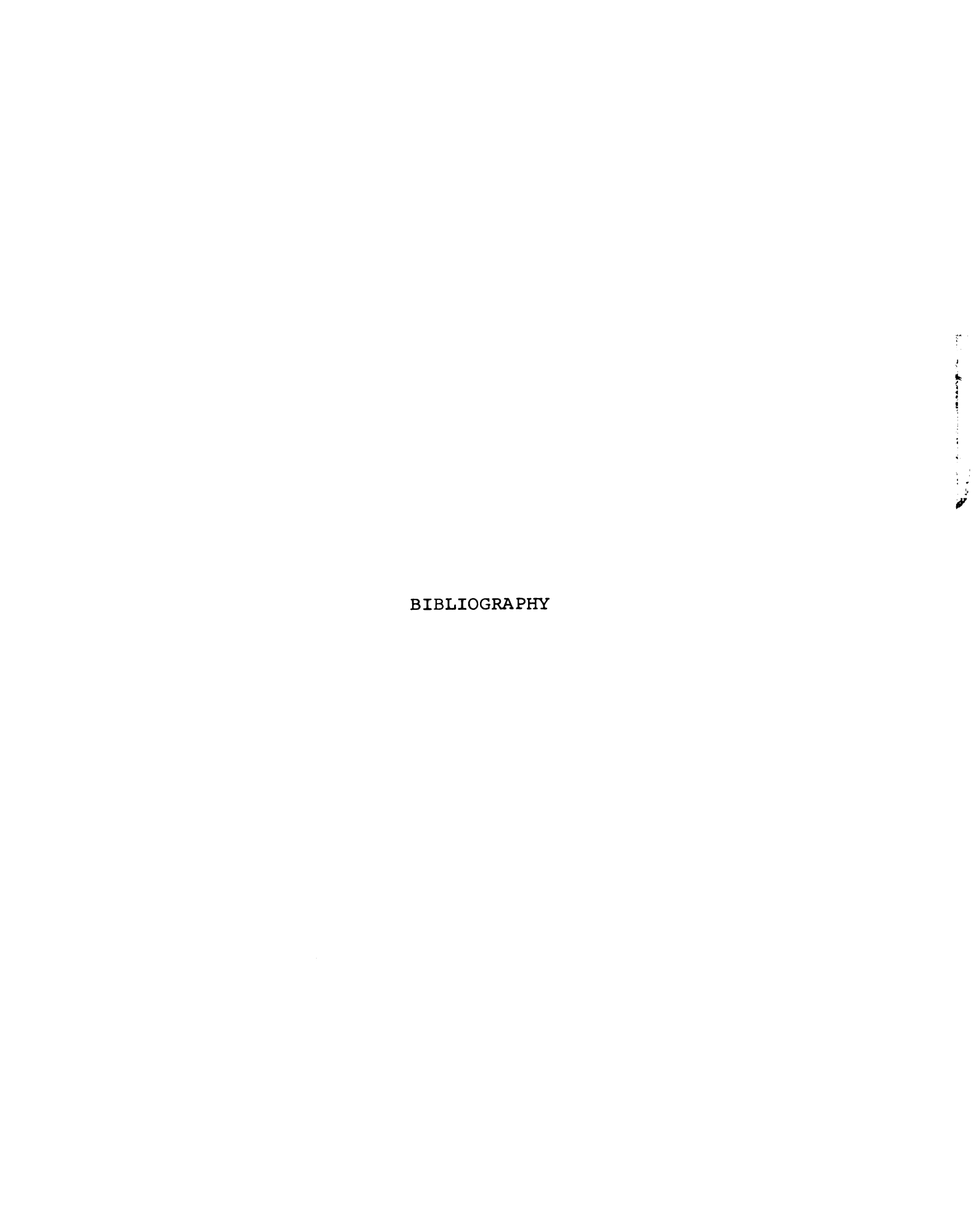
at this temperature the bomb will generally expand to its full size. Subsequently, cool the bomb and reposition the heating coil to adjust the temperature gradient. A ten centimeter long bomb with its bottom end at the center of a twenty to twenty-five centimeter coil appears to produce a reasonable gradient. Heat the sample portion of the vapor transport bomb to 1200-1400° for twelve to twenty-four hours and then cool it in a stepwise manner over about a fourty-eight-hour interval. This heating procedure should produce well annealed single crystals. The bombs may be opened in air (standard tubing cutter applied near the center of the bomb) and the vapor transport product removed by scraping. The product should be maintained under paraffin oil since hydrolysis occurs on prolonged exposure to air.

The composition of the bulk sample should be samarium deficient with respect to the desired composition of the crystal. The high samarium content of the condensate found on the vacuum line walls after an open bomb was heated indicates that the vapor contains a higher samarium to fluorine ratio than the residue. A mass spectrometric determination of this ratio as a function of composition would facilitate selection of the composition of the starting samples.

A series of crystals should be examined to provide an understanding of the structural aspects of this system. These should include: $SmF_{2.16}$, the nature of which is unknown in both systems; $SmF_{2.25}$, to establish the existence

of a distinct phase and determine its structure; $SmF_{2.33}$, to determine the true symmetry of the unit cell, $SmF_{2.41}$, to establish the relationship of this phase to $SmF_{2.50}$; and $SmF_{2.50}$ to establish this crystal structure and compare its co-ordination with that in SmF_3 . The complexity of the oxygen-rich portion of the uranium oxide system may establish merit for additional investigation of the analogous region in the samarium system.

Accomplishment of this suggested research represents a considerable expenditure of effort but should contribute substantially to an understanding of the anion rich behavior of the fluorite lattice and consequently serve as a model for the description of other related chemical systems.



BIBLIOGRAPHY

- 1) E. M. Brainina, R. Kh. Freidlina, and A. N. Nesmeyanov, Dokl. Akad. Nauk SSSR, (Eng. Transl.) 138, 628 (1961).
- 2) E. M. Brainina, R. Kh. Freidlina, and A. N. Nesmeyanov, ibid., (Eng. Transl.) 154, 143 (1964).
- 3) E. M. Brainina and R. Kh. Freidlina, <u>Izv. Akad. Nauk</u> <u>SSSR, Ser. Khim.</u>, <u>1964</u>, <u>1421</u>; <u>Chem. Abstr. 64</u>, <u>14214</u>c (1966).
- 4) J. C. Thomas, Chem. and Ind., 1956, 1388.
- 5) G. Wilkinson and F. A. Cotton, <u>Progress in Inorganic Chemistry</u>, Vol. I, Interscience Publishers, New York, 1959, pp 1-124.
- 6) F. A. Cotton, <u>Chemical Applications of Group Theory</u>, Interscience Publishers, New York, N.Y., 1963, pp 177-180.
- 7) R. J. Doedens and L. F. Dahl, <u>J. Am. Chem. Soc.</u>, <u>87</u>, 2576 (1965).
- 8) F. A. Cotton and G. Wilkinson, Advanced Inorganic Chemistry, 2nd ed, Interscience Publishers, New York, N.Y., 1966, pp 664-668.
- 9) R. J. H. Clark, D. L. Fepert, R. S. Nyholm, and J. Lewis, <u>Nature</u>, <u>199</u>, 559 (1963).
- 10) E. C. Lingafelter and R. L. Braun, <u>J. Am. Chem. Soc.</u>, 88, 2951 (1966).
- 11) T. J. Pinnavaia, J. J. Howe, and A. D. Butler, <u>ibid.</u>, 90, 5288 (1968).
- 12) G. Doyle and R. S. Tobias, Inorg. Chem., 6, 1111 (1967).
- 13) M. Straumanis and A. Ievins, Z. Phys., 102, 353 (1936).
- 14) E. W. Washburn, Ed., <u>International Critical Tables of Numerical Data</u>, <u>Physics</u>, <u>Chemistry</u>, <u>and Technology</u>, Vol. III, McGraw-Hill Book Co., Inc., New York, N.Y., 1928, pp 28.

- 15) C. H. MacGillavry, G. D. Reick, and K. Lonsdale, Eds., <u>International Tables for X-ray Crystallography</u>, Vol. III, The Kynoch Press, Birmingham, England, 1962, pp 166.
- 16) P. Coppens, L. Leiserowitz, and Rabinovich, Acta Cryst., 18, 1035 (1965).
- 17) W. R. Busing and H. A. Levy, <u>ibid</u>., 10, 180 (1957).
- 18) D. B. Shinn, Ph.D. Thesis, Michigan State University, East Lansing, Mich., 1968, pp 115-119.
- 19) L. H. Thomas and K. Umeda, <u>J. Chem. Phys.</u>, <u>26</u>, 293 (1957).
- 20) J. Berghuis, M. Haanapel, M. Potters, E. O. Loopstra,
 C. H. MacGillavry, and A. L. Veenendaal, Acta Cryst.,
 8, 478 (1955).
- 21) E. W. Hughes, J. Am. Chem. Soc., 63, 1737 (1941).
- 22) R. C. Weast, Ed., <u>Handbook of Chemistry and Physics</u>, 45th ed, Chemical Rubber Co., Cleveland, O., 1964, pp E-72.
- 23) D. T. Cromer and J. T. Waber, Acta Cryst., 18, 104 (1965).
- 24) J. V. Silverton and J. L. Hoard, Inorg. Chem., $\frac{2}{2}$, 243 (1963).
- 25) L. Pauling, <u>The Nature of the Chemical Bond</u>, **3**rd ed., Cornell University Press, Ithaca, N.Y., 1960, p 260.
- 26) G. L. Glen, J. V. Silverton, and J. L. Hoard, <u>Inorg.</u>
 <u>Chem.</u>, 2, 251 (1963).
- 27) R. D. Burbank and F. N. Bensey, <u>U. S. Atomic Energy</u> Comm., Report No. K-1280, (1956).
- 28) H. Bode and G. Tuefer, Acta Cryst., 9, 929 (1956).
- 29) J. L. Hoard and J. V. Silverton, Inorg. Chem., $\frac{2}{2}$, 235 (1963).
- 30) W. H. Zachariasen, Acta Cryst., 2, 288 (1949).
- 31) W. H. Zacharaisen, ibid., 1, 265 (1948).
- 32) G. Duffey, <u>J. Chem. Phys.</u>, <u>18</u>, 746 (1950).
- 33) G. Duffey, <u>ibid</u>., <u>18</u>, 1444 (1950).
- 34) G. Racah, <u>ibid</u>., 11, 214 (1943).

- 35) D. L. Kepert, J. Chem. Soc., 1965, 4736.
- 36) R. V. Parish and P. G. Perkins, <u>J. Chem. Soc.</u>, 1967A 345.
- 37) B. G. Hyde, D. J. M. Bevan, and L. Eyring, <u>Phil. Trans</u>. Roy. Soc., A259, 583 (1966).
- 38) L. Eyring and N. C. Baenziger, <u>J. Appl. Phys. Suppl.</u>, 33, 428 (1962).
- 39) J. O. Sawyer, B. G. Hyde, and L. Eyring, <u>Bull. Soc.</u> <u>Chim. Fr.</u>, 1956, 1190.
- 40) D. B. Shinn, Ph.D. Thesis, Michigan State University, East Lansing, Mich., 1968, pp 62-104.
- 41) L. R. Batsanova and G. N. Kustova, Russ. J. Inorg. Chem., (Eng. Transl.), 9, 181 (1964).
- 42) W. H. Zachariasen, Acta Cryst., 4, 231 (1951).
- 43) G. Brauer and U. Roether, presented in part at the <u>VII</u>
 <u>Earth Research Conference</u>, Coronado, Calif., Oct. 1968.
- 44) L. B. Asprey, F. H. Ellinger, and E. Staritzky, Rare Earth Research II, K. S. Vorres, Ed., Gordon and Beach, N.Y., 1964, pp 11-20.
- 45) R. M. Dell, <u>Reactivity of Solids</u>, G. M. Schwab, Ed., Elsevier Publishing Co., N.Y., 1965, pp 202-203.
- 46) H. Hering and P. Perio, Bull. Soc. Chim. Fr., 1952, 351.
- 47) A. D. Kirshenbaum and J. A. Cahill, <u>J. Inorg. Nucl. Chem.</u>, 14, 148 (1960).
- 48) P. G. Hambling, Acta Cryst., 6, 981 (1953).
- 49) O. Lindqvist and F. Wengelin, Ark. Kemi, 28, 179 (1967).
- 50) A. Zalkin and D. H. Templeton, <u>J. Am. Chem. Soc.</u>, <u>75</u>, 2453 (1953).
- 51) I. Oftedal, <u>Z. physik Chem.</u>, <u>B5</u>, 272 (1929); <u>B13</u>, 190 (1931).
- R. C. Weast, Ed., <u>Handbook of Chemistry and Physics</u>, 45th ed. Chemical Rubber Co., Cleveland, O., 1964, pp F-4.
- 53) L. Pauling, <u>The Nature of the Chemical Bond</u>, Cornell University Press, Ithaca, N.Y., 1960, pp 507-537.

- 54) D. H. Templeton and C. H. Dauben, <u>J. Am. Chem. Soc.</u>, 76, 5237 (1954).
- 55) H. A. Eick, N. C. Baenziger, and L. Eyring, <u>ibid</u>., <u>78</u>, <u>147</u> (1956).
- 56) K. Lee, H. Muir, and E. Catalano, <u>J. Phys. Chem. Solids</u>, 26, 523 (1965).
- 57) E. Catalano and R. Bedford, personal communication, University of California, Livermore, Calif., 1968.
- 58) L. Lynds, W. A. Young, J. S. Mohl, and G. G. Libowitz, 1963, Advances in Chemistry Series, 39, 58 (1963).
- 59) B. Belbeoch, C. Piekarski, and P. Pério, Acta Cryst., 14, 837 (1961).
- 60) E. S. Makarov, <u>Dokl. Akad. Nauk SSSR</u>, (Eng. Transl.), 139, 720 (1961).
- 61) H. R. Hoekstra, A. Santoro, and S. Seigel, <u>J. Inorg.</u>
 Nucl. Chem., 18, 166 (1961).

APPENDIX I

DESCRIPTION OF COMPUTER PROGRAM

APPENDIX I

DESCRIPTION OF COMPUTER PROGRAM

Program Distan

Program Distan written by A. Zalkin and modified by Lundgren and Luminga, calculates interatomic distances, bond angles, and their standard deviations. This program also calculates the thermal motion effects associated with the temperature factors.

A. Interatomic Distances

Interatomic distances are calculated from the position co-ordinates (X,Y,Z) in an oblique co-ordinate system $(A,B,C,\alpha,\beta,\gamma;$ i.e. a triclinic unit cell) by application of the following equation:

$$d = (d_X^2 + d_Y + d_Z + 2d_Yd_Z \cos \alpha + 2 d_Xd_Y \cos \beta + 2 d_Xd_Y \cos \gamma)^{1/2}$$
 where
$$d_Y = (X_2 - X_1)A, \quad \underline{\text{etc.}}$$

B. Standard Deviations in Interatomic Bond Distances

Standard deviations are calculated as the sum of independent components. The contributions due to the standard
deviations in the lattice parameters and the position coordinates are determined separately and then combined
according to the equation:

$$\sigma = \left(\sum_{i} \sigma_{i}^{2}\right)^{1/2}$$

The standard deviation of the interatomic distance due to the variation in the lattice parameters is

$$\sigma_{L.P.} = S_A^2 + S_B^2 + S_C^2 + S_\alpha^2 + S_\beta^2 + S_\gamma^2$$

where

$$S_{A} = (X_2 - X_1)(d_x + d_z \cos \beta + d_y \cos \gamma)\frac{\sigma_A}{d}, \quad \sigma_A =$$

standard deviation in the A lattice parameter, and

$$S_{\alpha} = -(d_{x}d_{z} \sin \alpha) - \frac{\sigma_{\alpha}}{d}$$
, $\sigma_{\alpha} = \text{standard deviation in angle}$

The component resulting from variations in the atomic position co-ordinates

$$\sigma_{P.C.} = \sum_{i=1}^{2} (S_{x_{i}}^{2} + S_{y_{i}}^{2} + S_{z_{i}}^{2} + 2S_{x_{i}}^{S} S_{y_{i}}^{S} \cos \gamma^{*} + 2S_{x_{i}}^{S} S_{z_{i}}^{S} \cos \alpha^{*})$$

$$+ 2S_{x_{i}}^{S} S_{z_{i}}^{S} \cos \beta^{*} + 2S_{y_{i}}^{S} S_{z_{i}}^{S} \cos \alpha^{*})$$

where

$$S_{x_i} = (d_x A + d_y A \cos \gamma + d_z A \cos \beta) \frac{\sigma_{x_i}}{d}$$
 and

 $\sigma_{\mathbf{x}_{i}}$ = standard deviation in the \mathbf{x}_{i} position co-ordinate.

Space group translations and symmetry elements also govern the manner in which the standard deviation in the position parameters effect the variation in the bond distances.

Translation Related Elements:

$$S_{X_2}' = 2S_{X_2}$$
 and $S_{X_1}' = 0$

<u>i.e.</u> Atom (1) is considered to be a stationary point and its standard deviation is added to that of the second atom.

For high symmetry space groups, (hexagonal, rhombohedral, tetragonal, and cubic) the translation equations result in an exchange of co-ordinates (i.e. X = Y). These translations produce the following equations

$$S'_{x_{i}} = 2S_{x_{i}}$$
 and $S'_{y_{i}} = 0$,

and for symmetry such that $y_i = 2x_i$

$$s'_{x_i} = 3s_{x_i}$$
 and $s'_{y_i} = 0$.

Cubic and rhombohedral space groups impose similar requirements on $\mathbf{S_{z}}_{i}$ and they are also related to $\mathbf{S_{x}}_{i}$. Therefore, standard deviations in the bond distances between symmetry related atoms is larger than it is for symmetry independent atoms.

C. Thermal Motion: Uncertainty, and its Effects on Bond Distances

The thermal parameters, isotropic or anisotropic, also effect the probability of locating an atom at a given point. Since these parameters adjust the atomic scattering factors for temperature effects, they are generally considered to reflect thermal motion of the atoms.

The error associated with these parameters (root-mean-square-error) is calculated from the equations:

a) Isotropic thermal parameters:

$$\bar{\mathbf{U}}_{i} = \left(\frac{\mathbf{B}_{iso}}{8\pi^{2}}\right)^{1/2}$$

b) Anisotropic thermal parameters:

$$\bar{U}_{A} = \left(\frac{B_{11}A^{2} + B_{22}B^{2} + B_{33}C^{2} + B_{12}AB\cos \gamma + B_{13}AC\cos \beta + B_{23}BC\cos \alpha}{6 \pi^{2}}\right)^{1/2}$$

Further application of the concept of thermal motion is made to determine the increase in the bond length as a result of a) motion of one atom with respect to the other or b) independent motion of both atoms.

Relative Thermal Motion:

a) Isotropic

$$M_{d_{\hat{1}}} = 2 \Delta \bar{u}_{\hat{1}}/3$$

$$\Delta d = M_{d_{\hat{2}}} - M_{d_{\hat{1}}}$$

$$d_{1,2} = d + \frac{\Delta d}{2d}$$

b) Anisotropic

$$\Delta X_{a} = (d_{x} + d_{z} \cos \beta + d_{y} \cos \gamma) \frac{A}{d}$$

$$M_{d_{a}} = (\Delta X_{a}^{2} B_{11} + \Delta Y_{a}^{2} B_{22} + \Delta Z_{a}^{2} B_{33} + \Delta X_{a} \Delta Y_{a} B_{12} + \Delta X_{a} \Delta Z_{a} B_{13} + \Delta Y_{a} \Delta Z_{a} B_{23})/2\pi^{2}$$

$$\Delta d = \Delta M_{d_{a}}$$

$$d_{1,2} = d + \frac{\Delta d}{2d}.$$

The value $d_{1,2}$ is the bond distance between two atoms

when one atom is in motion. The atom with the smaller $\mathbf{M}_{\mathbf{d}_i}$ (thermal motion) is considered to be the stationary atom.

Independent Thermal Motion:

When both atoms are considered to be in motion the bond length may be obtained from the equation:

$$d_{ind} = d + \frac{M_{d_1} + M_{d_2}}{2d}$$

where M_{d_1} and M_{d_2} are obtained from either the isotropic or anisotropic thermal parameters.

D. Angles

The "bond" angles, determined when two or more different atoms are considered to be bound to another atom, may also be determined from the calculated interatomic distances. The problem reduces to the determination of an angle in a Euclidian triangle by application of the Law of Cosines:

$$\cos^{-1} \phi = (d_1^2 + d_2^2 - d_3^2)/2d_1d_2$$

The standard deviations in the angles are determined by an extension of the standard deviation calculations, described previously, to include three distances and the magnitude of the angle.

Similar symmetry considerations are also made for symmetry related atoms.

Least Squares Plane and Line Fitting Program

This program fits a least squares plane or line to a selected set of rigid points (atoms) and determines the standard deviation of the plane or line independently of the variations in the lattice parameters or position co-ordinates. The program, outlined here, is an application of the method suggested and described in detail by Schomaker et al.¹

Least Squares Plane:

The points are considered as vectors of the form $r = x_1\bar{a}_1 + x_2\bar{a}_2 + x_3\bar{a}_3 \quad \text{and a general plane is defined by }$ the equation of its normal:

$$\bar{m} = m_1 \bar{b}_1 + m_2 \bar{b}_2 + m_3 \bar{b}_3$$

Vector \bar{m} can be converted to a unit matrix by matrix multiplication with matrix G_{ij} . A second matrix A_{ij} is set up from the co-ordinates of the atoms. This matrix consists of elements referenced to a new origin which is the centroid determined from the co-ordinates of the atoms.

The vector $\overline{\mathbf{m}}$ may be represented by a three element column matrix, for which

$$A_{ij} m_{j} = \lambda g_{ij} m_{j} \qquad i = 1,2,3$$

represents the minimum in the standard deviation from the general plane, and $\,\lambda\,$ is a Legrange multiplier.

The solution to the above equation, which is cubic in λ , produces three roots $\lambda_1 << \lambda_2 \leq \lambda_3$ corresponding to

the best plane, an intermediate plane, and the worst plane, all at right angles to one another and all passing through the centroid. An exact plane corresponds to $\lambda_1=0$, and thus the smaller λ_1 is, the more co-planar the atoms are.

The solution to standard eigenvalue problems requires solution of the cubic equation and a set of simultaneous linear equations for the components of the eigenvectors. When λ_1 is small this solution may be approximated by an iteration technique. This iteration is effected with the equation

$$B_{ij} m_{j} = \hat{A}_{ij} g_{ij} m_{j}$$

where \hat{A}_{ij} is the adjoint of A_{ij} . The successive matrix multiplication and the solution of its determinant refines the vector coefficients m_{ij} for the equation of the plane.

Least Squares Line:

The technique used for the generation of a least squares line is similar to that for the plane except that the best line is perpendicular to the worst plane, eigen value λ_3 . Therefore, a good fit to a line requires $\lambda_3 >> \lambda_2$, λ_1 . This fit is effected with matrix g_{ij}^{-1} A_{ij} rather than with B_{ij} . The equation generated by this technique is of the form:

$$\bar{r} = \bar{r}_{centroid} + tm_3$$

where t is a constant.

V. Shomaker, G. Wasser, R. E. Marsh and G. Bergman, Acta Cryst., 12, 600(1959).

APPENDIX II

PARAMETERS FROM THE ANISOTROPIC REFINEMENT OF THE STRUCTURE OF $\pi\text{-C}_5\text{H}_5\left(\text{C}_5\text{H}_7\text{O}_2\right)_2\text{ZrCl}$

Table XVI. Atomic co-ordinates for $\pi - C_5H_5(C_5H_7O_2)_2$ ZrCl from the structure refinement with anisotropic thermal factors

Atom	X	Y	Z
Z r	0.0440	0.1656	0.1414
cl	0.3359	0.1007	0.1652
C_1	-0.0515	0.0030	0.1188
\mathtt{C}_{2}	-0.2141	0.0538	0.0764
C ₃	-0.2213	0.0992	0.1512
C4	-0.0410	0.0836	0.2551
C ₅	0.0934	0.0306	0.2337
01	-0.1702	0.2662	0.0956
02	-0.0910	0.1620	0.9757
C ₆	-0.2595	0.1922	0.7917
C ₇	-0.2110	0.2196	0.9005
C ₈	-0.2916	0.2882	0.9144
C ₉	-0.2718	0.3081	0.0074
C ₁₀	-0.3671	0.3904	0.0184
03	0.1672	0.2765	0.1191
04	0.1884	0.2240	0.2929
C ₁₁	0.2547	0.4259	0.1172
C ₁₂	0.2239	0.3507	0.1668
C ₁₃	0.2689	0.3644	0.2683
C ₁₄	0.2490	0.3029	0.3260
C ₁₅	0.3072	0.3172	0.4393

108
Table XVII. Anisotropic thermal parameters.

Atom	B ₁₁	B ₂₂	B ₃₃	B ₁₂	B ₁₃	B ₂₃
Zr	4.21	4.97	3.84	0.00	-1.86	-0.05
Cl	4.54	6.54	4.89	-0.15	-2.06	-0.18
C_1	6.01	7.13	7.28	-0.38	-3.06	1.06
\mathtt{C}_{2}	7.11	2.19	7.31	0.15	-4.28	0.33
C ₃	8.13	6.68	7.18	2.07	-5.48	-1.60
C_4	7.71	6.77	9.99	0.96	-7.33	1.00
C ₅	5.94	8.70	4.35	-0.12	-2.96	1.09
01	3.53	4.40	3.49	0.33	-1.04	-1.02
02	4.99	4.72	3.73	0.16	-2.44	0.26
C ₆	5.98	8.26	3.62	0.51	-3.09	0.05
C ₇	3.99	3.47	4.55	0.54	-0.91	0.47
C ₈	5.56	4.67	3.26	-1.59	-2.34	0.58
C ₉	2.93	9.06	2.50	2.45	0.66	-1.29
C ₁₀	6.13	3.14	8.08	-2.35	-2.95	1.65
03	3.67	6.39	4.39	0.36	-2.47	-1.22
04	4.96	4.63	3.92	-0.42	-1.74	-0.32
C_{11}	8.43	5.54	8.69	0.65	-3.94	2.29
C_{12}	3.48	6.99	3.85	-0.26	-1.93	-0.34
C ₁₃	2.90	7.39	3.49	-1.01	-0.76	1.09
C ₁₄	4.47	4.44	3.85	-0.97	-1.45	-1.26
C ₁₅	4.84	6.26	3.37	0.26	-1.74	-1.92

APPENDIX III

POWDER X-RAY DIFFRACTION DATA FOR THE $Sm(II)-Sm(III) \ FLUORIDES$

Table XVIII. Powder X-ray diffraction data for the cubic Sm(II)-Sm(III) fluorides.

109

	Sin ² θ		$\sin^2 \theta$	θ	
h k l	SmF _{1.83}	SmF _{2.00}	SmF _{2.01}	SmF _{2.01}	
1 1 1	0.05166	0.05170	0.05174	0.05168	
2 0 0	0.06892	0.06890	0.06892	0.06888	
2 2 0	0.13772	0.13785	0.13789	0.13775	
3 1 1	0.18948	0.18946	0.18958	0.18960	
2 2 2	0.20659	0.20679	0.20684	0.20678	
4 0 0	0.27545	0.27560	0.27595	0.27570	
3 3 1	0.32739	0.32760	0.32757	0.32761	
4 2 0	0.34478	0.34483	0.34492	0.34485	
4 2 2	0.41359	0.41349	0.41346	0.41352	
	SmF _{2.04}	SmF _{2.07}	SmF _{2.10}	SmF _{2.14}	
1 1 1	0.05171	0.05180	0.05190	0.05210	
2 0 0	0.06892	0.06914	0.06918	0.06940	
2 2 2	0.13802	0.13812	0.13832	0.013867	
3 1 1	0.18977	0.19026	0.19046	0.19076	
2 2 2	0.20709	0.20745	0.20765	0.20796	
4 0 0	0.27612	0.27682	0.27701	0.27757	
3 3 1	0.32757	0.32847	0.32927	0.32986	
	0.34484	0.34539	0.34609	0.34740	
4 2 0	0.34464	0.00.000			

Table XIX. Powder X-ray diffraction data for the samples in the cubic-tetragonal two-phase region.

h k &	$\mathtt{Sin^2}$ $ heta$	
bic Phase		
1 1 1	0.05207(10)*	
2 0 0	0.06946(15)	
2 2 0	0.13880(20)	
3 1 1	0.19125(40)	
tragonal Phase		
1 0 1	0.05265(10)	
0 0 2	0.06895(12)	
1 1 0	0.07055(10)	
1 1 2	0.14049(10)	
2 0 0	0.14097(5)	
1 0 3	0.19377(20)	
2 0 0	0.21086(20)	
2 1 3	0.33481(30)	
3 0 1	0.33523(30)	

^{*} Values in parentheses are the average deviations from three different products.

Table XX. Powder X-ray diffraction data for the tetragonal $SmF_{2.35}$ with the superstructure lines also included.

h k l	$\mathtt{Sin^2}$ $ heta$
	0.04510
	0.04665
1 0 1	0.05271
0 0 2	0.06990
1 1 0	0.07058
	0.07666
	0.07783
1 1 1	0.08783
	0.08911
	0.09775
1 0 2	0.10316
	0.10919
	0.12686
	0.13089
1 1 2	0.14002
2 0 0	0.14100
	0.15208
0 0 3	0.15587
	0.19061
1 0 3	0.19209
2 1 1	0.19367
2 0 2	0.21081
2 2 2	0.28162
	0.32874
2 1 3	0.33328
	0.35817

Table XXI. Powder X-ray diffraction data for the rhombohedral Sm(II)-Sm(III) fluorides.

	\mathtt{Sin}^{2} $ heta$		
h k l	SmF _{2.41}	SmF _{2.44}	SmF _{2.46}
0 0 6	0.05241	0.05238	0.05243
0 1 2	0.05311	0.05322	0.05327
1 0 4	0.07049	0.07045	0.07078
0 1 8	0.14058	0.14045	0.14071
1 1 0	0.14158	0.14171	0.14241
1 0 10		0.19273	0.19317
1 1 6	0.19406	0.19406	0.19471
2 0 2	0.19441	0.19491	0.19659
0 0 2	0.21015	0.2990	0.21004
0 1 14	0.33334	0.33358	0.33499
2 10	0.33452	0.33564	0.33795

